JOURNAL OF GEOPHYSICAL RESEARCH, VOL. 114, B01203, doi:10.1029/2008JB005900, 2009

The $MgSiO_3$ system at high pressure: Thermodynamic properties of perovskite, postperovskite, and melt from global inversion of shock and static compression data

Jed L. Mosenfelder,[1] Paul D. Asimow,[1] Daniel J. Frost,[2] David C. Rubie,[2] and Thomas J. Ahrens[1,3]

Received 26 June 2008; accepted 3 November 2008; published 14 January 2009.

[1] We present new equation-of-state (EoS) data acquired by shock loading to pressures up to 245 GPa on both low-density samples ($MgSiO_3$ glass) and high-density, polycrystalline aggregates ($MgSiO_3$ perovskite + majorite). The latter samples were synthesized using a large-volume press. Modeling indicates that these materials transform to perovskite, postperovskite, and/or melt with increasing pressure on their Hugoniots. We fit our results together with existing *P-V-T* data from dynamic and static compression experiments to constrain the thermal EoS for the three phases, all of which are of fundamental importance to the dynamics of the lower mantle. The EoS for perovskite and postperovskite are well described with third-order Birch-Murnaghan isentropes, offset with a Mie-Grüneisen-Debye formulation for thermal pressure. The addition of shock data helps to distinguish among discrepant static studies of perovskite, and for postperovskite, constrain a value of K' significantly larger than 4. For the melt, we define for the first time a single EoS that fits experimental data from ambient pressure to 230 GPa; the best fit requires a fourth-order isentrope. We also provide a new EoS for Mg_2SiO_4 liquid, calculated in a similar manner. The Grüneisen parameters of the solid phases decrease with pressure, whereas those of the melts increase, consistent with previous shock wave experiments as well as molecular dynamics simulations. We discuss implications of our modeling for thermal expansion in the lower mantle, stabilization of ultra-low-velocity zones associated with melting at the core-mantle boundary, and crystallization of a terrestrial magma ocean.

Citation: Mosenfelder, J. L., P. D. Asimow, D. J. Frost, D. C. Rubie, and T. J. Ahrens (2009), The $MgSiO_3$ system at high pressure: Thermodynamic properties of perovskite, postperovskite, and melt from global inversion of shock and static compression data, *J. Geophys. Res.*, *114*, B01203, doi:10.1029/2008JB005900.

1. Introduction

[2] Recent advances in geophysics and mineral physics have shed new light on processes occurring in the lower mantle of the Earth. Particularly exciting progress has been made in interpreting seismic anomalies and predicting dynamic behavior from the top of the D″ layer down to the core-mantle boundary (CMB). Anomalies associated with D″ have been popularly explained by the recently discovered perovskite to postperovskite phase transition in $(Mg,Fe)SiO_3$ [*Murakami et al.*, 2004; *Oganov and Ono*, 2004; *Hirose*, 2006], which was predicted by the seismological study of *Sidorin et al.* [1999]. At the CMB, another hypothesis [*Williams and Garnero*, 1996] calls upon the existence of dynamically stable partial melt to explain the presence of ultra-low velocity zones (ULVZ). The putative melt can be approximated as a eutectic composition between (Mg, Fe)O and $(Mg, Fe)SiO_3$. A basal melt layer at the CMB could also be the remnant of a more extensive magma ocean formed early in Earth's history, with attendant implications for the evolution of geochemical reservoirs in the planet [*Labrosse et al.*, 2007]. More accurate knowledge of the high-pressure and high-temperature behavior of solid and liquid phases in the $(Mg, Fe)SiO_3$ system is therefore of obvious interest for constraining processes that occur in the deep Earth.

[3] Although the thermal equation of state (EoS) of $MgSiO_3$ perovskite has been studied repeatedly via static compression, spectroscopy, and computational methods, significant discrepancies among different studies remain unresolved. In particular, agreement has only recently been reached on the value of the bulk modulus ($K_{0S} = 253(3)$ GPa) [*Sinogeikin et al.*, 2004; *Li and Zhang*, 2005; *Vanpeteghem et al.*, 2006], and the value of its pressure derivative (K'_{0S}) is still in dispute due to severe disagreement between the two highest-pressure static *P-V-T* studies [*Saxena et al.*, 1999; *Fiquet et al.*, 2000]. Moreover, published values of other

[1]Division of Geological and Planetary Sciences, California Institute of Technology, Pasadena, California, USA.
[2]Bayerisches Geoinstitut, Universität Bayreuth, Bayreuth, Germany.
[3]Lindhurst Laboratory of Experimental Geophysics, Seismological Laboratory, California Institute of Technology, Pasadena, California, USA.

0148-0227/09/2008JB005900$09.00

Table 1. Electron Microprobe Analyses[a]

	en97c[b] Glass (Four Analyses)	en99a[c] Glass (Three Analyses)	en07a[d] Glass (Four Analyses)	Z431[e] Perovskite (Three Analyses)
MgO	39.55(11)	38.53(34)	38.84(13)	42.06(36)
Al_2O_3	–	0.73(2)	–	0.19(7)
SiO_2	61.09(6)	60.38(42)	60.82(33)	62.43(49)
FeO	0.05(3)	–	–	–
Oxide totals	100.66(14)	99.69(70)	99.70(45)	104.73(47)
Mg	1.953(4)	1.920(7)	1.935(6)	2.002(18)
Al	–	0.029(1)	–	0.007(3)
Si	2.024(3)	2.018(4)	2.032(3)	1.993(8)
Fe	0.0015(9)	–	–	–
Cations per 6 O	3.978(2)	3.969(4)	3.969(2)	4.004(9)

[a]Dashes indicate that element was below the detection limit; Na, P, K, Ca, Ti, Ni, Mn, and Cr were also measured but were below the detection limit in all samples.
[b]Used for shots 365.
[c]Used for perovskite synthesis, see text.
[d]Used for shots 366,367, 369, and 370.
[e]Used for shot 366.

parameters, such as the coefficient of thermal expansion (α) and the temperature derivative of the bulk modulus ($\partial K/\partial T$), cover a wide range with no clear consensus at the present time. These thermal EoS parameters are essential for accurate modeling of the chemical composition and style of convection of the lower mantle [e.g., *Wang et al.*, 1994; *Anderson*, 1995; *Fiquet et al.*, 1998].

[4] The thermal EoS of $MgSiO_3$ postperovskite has so far only received serious attention from one experimental study [*Guignot et al.*, 2007] and two theoretical studies [*Ono and Oganov*, 2005; *Tsuchiya et al.*, 2005]. The high-precision data of *Guignot et al.* [2007] span a limited volume range due to the very high pressure of the phase transition and technical limitations of the laser-heated diamond anvil cell, requiring an assumption of $K' = 4$.

[5] In the case of high-pressure $MgSiO_3$ melt, the only available data come from shock wave experiments [*Akins et al.*, 2004; *Luo et al.*, 2004] and molecular dynamics simulations [*Belonoshko and Dubrovinsky*, 1996; *Stixrude and Karki*, 2005; *Wan et al.*, 2007]. Previous assessments of the EoS of the melt from shock experiments [*Akins et al.*, 2004; *Luo et al.*, 2004] described the data available at that time, but no attempt was made to reconcile the EoS with commonly used parameters estimated from regression of the partial molar 1 atm ($= 10^5 \times 1.01325$ N/m^2) properties of liquid oxides [*Lange and Carmichael*, 1990]. This implies a large discontinuity in thermodynamic properties that is inconsistent with the continuous change in melt structure and properties with compression documented by recent first-principles molecular dynamics simulations [*Stixrude and Karki*, 2005; *de Koker et al.*, 2008].

[6] Shock wave experiments have the potential to determine the thermal EoS at conditions complementary to those accessed by static experimental techniques and theoretical simulations. The bulk modulus K_{0S} and its pressure derivative K'_{0S} can be derived by reduction of shock data [e.g., *Jeanloz*, 1989], and the wider pressure and volume range that can be obtained by shock loading compared to static compression can provide tighter constraints on K'_{0S}. The Grüneisen parameter ($\gamma = V(\partial P/\partial E)_V$) is a thermodynamic entity that is directly determined by comparison of the Hugoniots of phases of identical composition but different initial density, because these materials obtain different internal energy states at equal volume upon shock compression [e.g., *Luo et al.*, 2002; *Mosenfelder et al.*, 2007]. This method of determining γ makes no assumption about heat capacity, since temperature is not one of the variables in reduction of shock EoS data. However, in combination with static *P-V-T* data and/or shock temperature measurements, γ and C_v can both be constrained as functions of volume.

[7] Methods for achieving different energy states off the principal Hugoniot of a phase include use of porous starting materials, preheated samples, and presynthesized high-pressure polymorphs. In this study, we present new EoS data acquired by shock loading of low-density samples ($MgSiO_3$ glass, $\rho_0 = 2.73$ Mg/m^3) and high-density, polycrystalline aggregates consisting of $MgSiO_3$ perovskite + majorite ($\rho_0 = 3.96–4.03$ Mg/m^3). The latter samples were recovered from high pressure and temperature in a multianvil device. Prior to destruction in the shock experiments, they were likely some of the largest volume aggregates of high-pressure $MgSiO_3$ polymorphs ever synthesized. The new results on these two materials are placed in the context of previous shock wave studies on crystalline enstatite, $MgSiO_3$ glass, and aggregates of variable porosity in the $MgSiO_3$ system, as well as *P-V-T* data from static compression. Assignment of the shock data to high-pressure phase regimes and global fitting of both shock and static data allows us to determine thermal EoS parameters for $MgSiO_3$ perovskite, postperovskite, and high-pressure $MgSiO_3$ melt.

2. Experimental Methods

2.1. Sample Synthesis and Characterization

[8] $MgSiO_3$ glass was synthesized as described by *Akins* [2003] and *Luo et al.* [2004]. Glass targets for shock wave experiments were prepared as rectangular plates, free of bubbles and cracks. Electron microprobe analyses of three different glasses used in this study are shown in Table 1. Sample densities (ρ_0) were measured via Archimedes' method using immersion in toluene (Table 2).

[9] We endeavored to synthesize large-volume, polycrystalline aggregates of pure $MgSiO_3$ perovskite using the 5000-tonne multianvil press in Bayreuth [*Frost et al.*, 2004]. Pressures and temperatures of approximately 22 GPa and 2073 K were generated at 1900 tonnes using an 18-mm assembly with a $LaCrO_3$ box-furnace design [cf. *Gwanmesia et al.*, 1993] and 8-mm truncation edge length WC cubes.

Table 2. Shock Data Used in This Study[a]

Starting Material	Reference	Shot	Flyer-Driver Material	U_{fp}, km/s	ρ_0, Mg/m^3	U_s, km/s	u_p, km/s	P, GPa	ρ, Mg/m^3	T_H, K	Phase State[b]
Pv77Mj23[c]	this study	370	Al 1100	6.13	3.970(21)	10.81(12)	2.42(2)	104.0(8)	5.12(3)		Pv
Pv77Mj23	this study	367	Cu	5.09	3.973(30)	11.76(16)	2.94(2)	137.4(15)	5.30(5)		Pv
Pv75Mj25	this study	366	Ta	5.17	3.958(13)	12.14(10)	3.41(2)	163.8(12)	5.51(3)		Pv
Pv86Mj14	this study	368	Cu	6.32	4.025(16)	12.71(14)	3.67(2)	187.4(17)	5.66(4)		Pv
Pv80Mj20	this study	369	Ta	6.96	3.989(12)	13.28(14)	4.63(2)	245.4(22)	6.13(5)		PPv
Glass	*Akins et al.* [2004]	313	Cu	5.05	2.743(2)	8.53(6)	3.55(1)	83.0(5)	4.70(3)		Pv
Glass	this study	367	Cu	5.09	2.731(1)	8.77(9)	3.56(1)	85.2(7)	4.59(4)		Pv
Glass	this study	366	Ta	5.17	2.731(1)	9.47(6)	3.93(1)	101.6(6)	4.67(3)		melt
Glass	*Akins* [2003]	311	Cu	5.97	2.737(2)	9.38(30)	4.17(3)	107.0(40)	4.92(10)	5050(173)	melt
Glass	*Akins et al.* [2004]	312	Cu	6.07	2.740(2)	9.49(13)	4.23(2)	110.0(12)	4.94(7)		melt
Glass	*Luo et al.* [2004]	335	Ta	5.67	2.747(2)	9.85(10)	4.30(2)	116.4(11)	4.88(5)	5580(130)	melt
Glass	*Luo et al.* [2004]	336	Ta	5.88	2.734(2)	9.92(16)	4.47(2)	121.0(17)	4.97(8)	5940(560)	melt
Glass	this study	365	Ta	6.20	2.741(1)	10.60(6)	4.66(1)	135.5(9)	4.90(3)		melt
Glass	this study	369	Ta	6.96	2.731(1)	11.20(10)	5.23(2)	160.0(12)	5.12(5)		melt
Enstatite	*Akins et al.* [2004]	326	Cu	5.44	3.199(9)	9.65(4)	3.59(1)	110.8(5)	5.09(2)		Pv
Enstatite	*Akins et al.* [2004]	316	Cu	5.71	3.199(9)	10.06(7)	3.75(1)	120.5(8)	5.10(3)		Pv
Enstatite	*Luo et al.* [2004]	340	Ta	5.85	3.199(9)	10.47(24)	4.26(2)	142.6(26)	5.39(10)	4130(50)	PPv
Enstatite	*Akins et al.* [2004]	321	Ta	5.98	3.199(9)	10.79(3)	4.33(1)	149.5(7)	5.34(2)		PPv
Enstatite	*Luo et al.* [2004]	341	Ta	6.38	3.199(9)	11.17(27)	4.61(3)	164.8(32)	5.45(11)	4900(140)	PPv
Enstatite	*Akins et al.* [2004]	324	Ta	6.52	3.199(9)	11.34(6)	4.71(2)	170.8(10)	5.47(3)		PPv
Enstatite	*Akins et al.* [2004]	318	Ta	6.71	3.199(9)	11.16(9)	4.87(2)	174.0(13)	5.68(5)		melt
Enstatite	*Luo et al.* [2004]	342	Ta	6.79	3.199(9)	11.59(28)	4.90(3)	181.6(35)	5.54(12)	5450(100)	PPv
Enstatite	*Akins et al.* [2004]	322	Ta	7.22	3.199(9)	11.69(5)	5.23(2)	195.5(10)	5.79(3)		melt
Enstatite	*Akins et al.* [2004]	319	Ta	7.38	3.199(9)	11.99(19)	5.33(2)	204.3(27)	5.76(9)		melt
Porous Enstatite	*Simakov and Trunin* [1973]				3.040	8.96	3.30	90(1)	4.81(5)		Pv
Porous Enstatite	*Simakov and Trunin* [1973]				3.040	9.59	3.70	108(1)	4.95(5)		Pv
Porous Enstatite	*Simakov and Trunin* [1973]				3.040	12.56	6.03	230(1)	5.85(6)		melt
Porous Enstatite [3.01][d]	*Marsh* [1980]				3.000	8.195	2.90	71.4(10)	4.647(46)		Pv
Porous Enstatite [3.01]	*Marsh* [1980]				3.011	8.192	2.93	72.2(10)	4.689(47)		Pv
Porous Enstatite [3.01]	*Marsh* [1980]				3.005	8.183	2.94	72.2(10)	4.686(47)		Pv
Porous Enstatite [3.01]	*Marsh* [1980]				3.006	9.083	3.38	92.4(10)	4.790(48)		Pv
Porous Enstatite [2.95]	*Marsh* [1980]				2.985	8.446	3.14	79.1(10)	4.748(47)		Pv
Porous Enstatite [2.95]	*Marsh* [1980]				2.951	8.933	3.43	90.4(10)	4.791(48)		Pv
Porous Enstatite [2.83]	*Marsh* [1980]				2.828	8.626	3.50	85.4(10)	4.761(48)		Pv
Porous Enstatite [2.83]	*Marsh* [1980]				2.827	9.086	3.74	96.1(10)	4.806(48)		Pv
Porous Enstatite [2.83]	*Marsh* [1980]				2.831	9.124	3.80	98.2(10)	4.854(49)		Pv
Porous Enstatite [2.83]	*Marsh* [1980]				2.833	9.162	3.87	100.3(10)	4.900(49)		Pv
Porous Enstatite [2.83]	*Marsh* [1980]				2.833	9.286	3.95	103.8(10)	4.926(49)		Pv
Porous Enstatite [2.76]	*Marsh* [1980]				2.759	8.905	3.83	94.0(10)	4.836(48)		Pv
Oxide mix	*Marsh* [1980]				1.560	6.164	3.52	33.9(10)	3.641(36)		melt
Oxide mix	*Marsh* [1980]				1.570	6.675	3.87	40.5(10)	3.733(37)		melt

[a]Uncertainties denoted in parentheses; uncertainty in U_{fp} for Caltech experiments is ±0.01 km/s.
[b]Phase state is the interpreted phase state on hugoniot (Pv is perovskite and PPv is postperovskite).
[c]"PvXMjX" denotes volume proportions of perovskite and majorite.
[d]Number in brackets is average density of series, for comparison to original tabulation.

Temperature was monitored using type D thermocouples. The starting material for each experiment was clinoenstatite, prepared by crystallizing $MgSiO_3$ glass (sample EN99A; Table 1) at 1 atm and 1773 K. The crystalline powder was packed into a Re capsule with an outer diameter of 3.3 mm, which was isolated from the $LaCrO_3$ furnace by an MgO sleeve. Following decompression over a period of ~17 hours and recovery, each disk-shaped sample was prepared by stripping off the Re foil capsule, cutting the irregularly shaped ends off with a wire saw, and polishing flat surfaces on each side of the sample. Typical final dimensions for the samples used in the shock wave experiments were 2.7 mm in diameter by 0.85 mm in thickness (Figure 1).

[10] The deficit between the theoretical density for $MgSiO_3$ perovskite (4.108 Mg/m^3) [*Horiuchi et al.*, 1987] and the actual sample densities (3.958–4.025 Mg/m^3; Table 2) cannot be caused by porosity, which was estimated at $\ll$1% by scanning electron microscope observation of recovered samples. Rather, it is explained by the presence of 14 to 25% (by volume) majorite, which was established using Raman spectroscopy (Figure 2). Bands at 254, 283, 342, 380, 499, 540, and 663 cm^{-1} in the spectra correspond to $MgSiO_3$ perovskite [*Durben and Wolf*, 1992], whereas the band near 931 cm^{-1} and the weak band near 600 cm^{-1} both correspond to majorite [*McMillan et al.*, 1989]. The small peak at 804 cm^{-1} could also be attributed to majorite, although a band near this location was also documented in Al-bearing $MgSiO_3$ perovskite samples by *Litasov et al.* [2003]. Note the lack of broad features centered at 650 cm^{-1} and 980 cm^{-1}, which are characteristic of amorphization [*Durben and Wolf*,

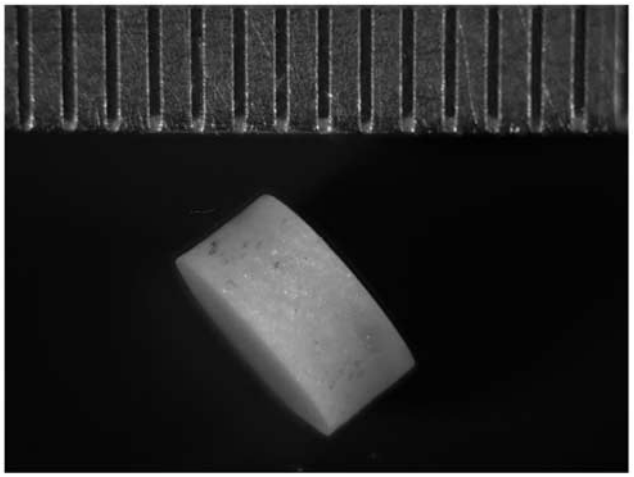

Figure 1. Photograph of synthetic perovskite (+majorite) aggregate, showing typical dimensions of recovered samples. Note lack of cracks. Grey specks are rhenium metal at the outer surface of the sample, left over after stripping the capsule foil. Ticks on scale bar are 0.5 mm.

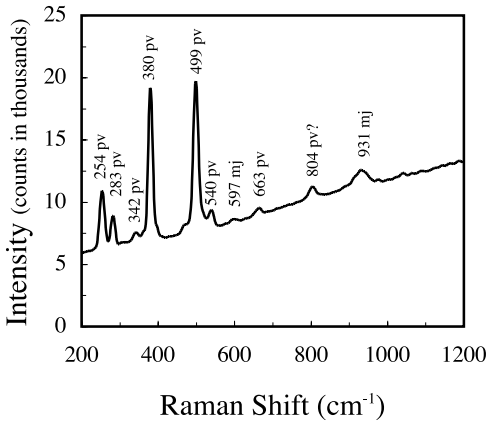

Figure 2. Representative Raman spectrum showing presence of perovskite + majorite in samples used for shock wave experiments. See text for discussion of band assignments.

1992]. The majorite bands at 600 and 931 cm^{-1} appear in most but not all spectra, which were collected with a laser spot size of about 2 μm.

[11] The majorite may be stabilized by the presence of alumina in the original starting material [e.g., *Akaogi and Ito*, 1999]. The glass used to make the clinoenstatite contained ~0.7 wt% Al_2O_3, whereas analyses of the recovered perovskite show lower concentrations of Al_2O_3 (~0.2 wt%) and insignificant concentrations of any other impurity (Table 1). Another possibility is that the majorite forms as a result of pressure decrease accompanying volume reduction during transformation [*Rubie*, 1999]. Formation due to temperature gradients is unlikely because the majorite phase is well distributed within the aggregates, according to Raman spectroscopic mapping. We emphasize that for the purposes of this study, it is more important that the initial density and phase proportions (hence internal energy) of each sample be accurately known than that the sample be pure perovskite phase.

2.2. Shock Wave Experiments

[12] Shock wave EoS experiments were performed with the light-gas gun at Caltech using the procedures outlined by *Mosenfelder et al.* [2007]. Shock wave velocities (U_s) were determined by analyzing digitized streak camera records and particle velocity (u_p), pressure (P_H), density (ρ_H), and internal energy (ΔE) at the peak shock state were calculated by impedance matching, using standard Hugoniot data for Ta, Cu, or Al1100 flyer and driver plates from *Mitchell and Nellis* [1981]. Uncertainties were evaluated using standard analytical error propagation, as in *Mosenfelder et al.* [2007]. The data are shown in Table 2 as well as Figures 3 and 4.

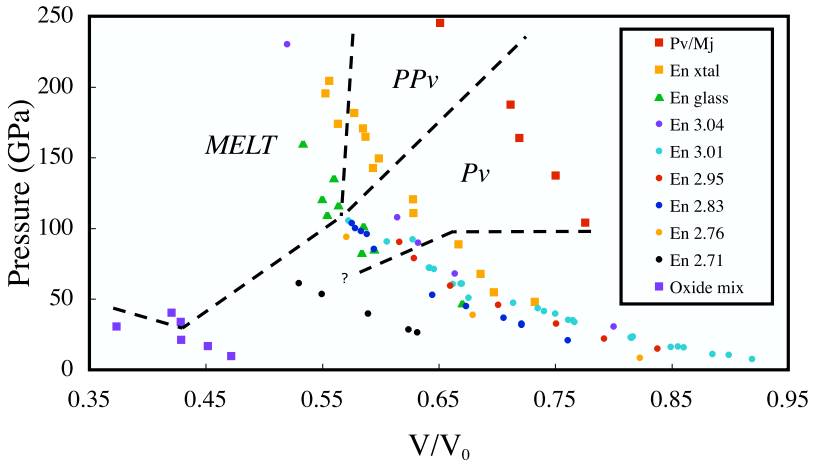

Figure 3. $MgSiO_3$ Hugoniot data. Volume for each datum is normalized to the volume of its respective starting material. Plot includes results on initial perovskite + majorite (this study), single crystal enstatite [*Akins*, 2003; *Akins et al.*, 2004; *Luo et al.*, 2004], glass (*Akins et al.* [2004], *Luo et al.* [2004], and this study), porous enstatite [*Simakov and Trunin*, 1973; *Marsh*, 1980], and porous oxide mix [*Marsh*, 1980]. Experiments on porous enstatite are subdivided by average density as shown in figure legend. High-pressure states assigned to either perovskite, postperovskite, or melt as shown by the dashed lines; data at lower pressures are assigned to mixed-phase regimes and/or lower pressure phases. For sake of clarity, error bars not shown.

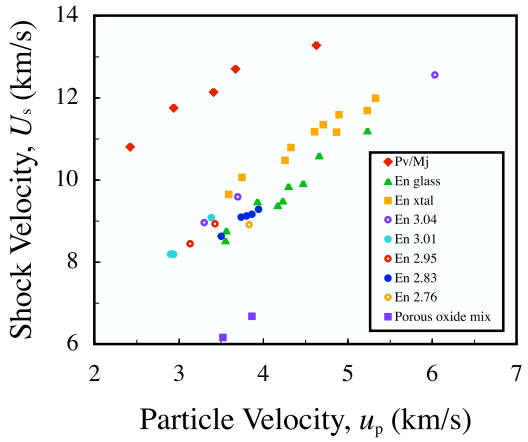

Figure 4. Shock velocity versus particle velocity, for data used in modeling (see Table 2). Same symbols and data sources as in Figure 3.

[13] Compared to the study of *Mosenfelder et al.* [2007], samples were typically 20% thinner, due to the necessity of maintaining a 3:1 aspect ratio in order to mitigate edge effects due to rarefaction from the sides of the sample. However, the writing rate of the streak camera was increased 31% by use of a new fast-streak optoelectronic unit, resulting in a net reduction in uncertainty for measured shock wave velocities.

3. Thermal Equations of State

[14] The details of data selection for our global inversion are discussed in sections 4 and 5. First, we specify our approach to modeling the data. For static *P-V-T* data on perovskite and postperovskite, we fit to a Mie-Grüneisen-Debye EoS:

$$P_{tot}(V,T) = P_S(V) + \Delta P_{th}(V,T). \tag{1}$$

The first term on the right-hand side is typically considered as an isotherm at T_0 = 0 or 300 K. In the present case, however, we fit an isentropic rather than isothermal Birch-Murnaghan EoS, and we consider both third- and fourth-order fits:

$$P_S = 3K_{0S}f(2f+1)^{5/2}\left(1+\frac{3}{2}\left[K'_{0S}-4\right]f\right), \tag{2}$$

$$P_S = 3K_{0S}f(2f+1)^{5/2}\left(1+\frac{3}{2}\left[K'_{0S}-4\right] \cdot f+\frac{3}{2}\left[K_{0S}K''_{0S}+K'_{0S}\left(K'_{0S}-7\right)+\frac{143}{9}\right]f^2\right), \tag{3}$$

where f (Eulerian strain) is

$$f = \left[(V_0/V)^{2/3}-1\right]/2 \tag{4}$$

and we emphasize that $K_{0S}{}'$ and $K_{0S}{}''$ are fully isentropic derivatives [see, e.g., *Anderson*, 1995, equation (1.59)]. In order to visualize the quality of fit of Birch-Murnaghan expressions we use *f-F* plots (Figure 5), where F (normalized stress) is defined as:

$$F = P/\left[3f(2f+1)^{5/2}\right] \tag{5}$$

The second term on the right-hand side of equation (3), accounting for thermal pressure, is [*Luo et al.*, 2003]

$$\Delta P_{\mathrm{th}}(V,T) = \frac{\gamma C_{vm}}{V}\left[TD\left(\frac{\theta}{T}\right) - T_0 D\left(\frac{\theta}{T_S}\right)\right], \tag{6}$$

where C_{vm} is the high-temperature limit of heat capacity, θ is the Debye temperature at volume V, T_{S} is the temperature along the reference isentrope at volume V, and the function

$$D(x) = \frac{3}{x^3}\int_0^x \frac{y^3 dy}{e^y - 1}. \tag{7}$$

Although C_{vm} is typically assumed to be the Dulong-Petit limit of 3nR for solids (where R is the gas constant and n is the number of atoms per formula unit, expressed in units of J K^{-1} g^{-1} for the sake of our calculations), we use it as a fit parameter along with θ_0 (the Debye temperature at ambient volume), γ, K_{0S}, K'_{0S}, and (for fourth-order fits) K''_{0S}. Thus V_0 is the only fixed parameter in our models for the EoS of perovskite and postperovskite. This distinguishes our modeling from previous global inversion efforts in which more parameters were fixed [*Bina*, 1995; *Jackson and Rigden*, 1996; *Shim and Duffy*, 2000; *Stixrude and Lithgow-Bertelloni*, 2005]. In the case of perovskite, we have renormalized all the volumes from static *P-V-T* data used in our modeling to a value of V_0 = 162.35 Å^3 [*Horiuchi et*

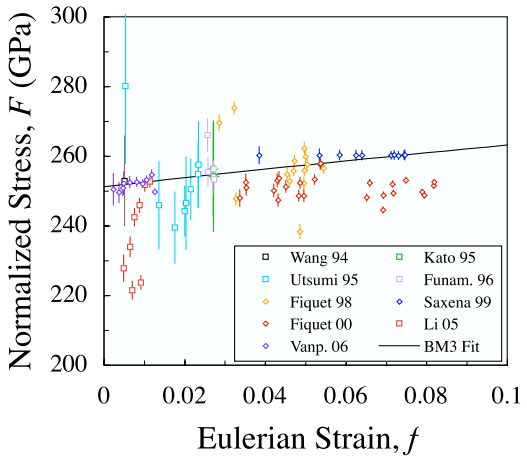

Figure 5. The *f-F* plot of selected room temperature (~300 K) static compression data on $MgSiO_3$ perovskite. At the highest pressures, the trend of the data of *Fiquet et al.* [2000] clearly diverges from that of *Fiquet et al.* [1998] and *Saxena et al.* [1999]. Curve corresponds to our third-order Birch-Murnaghan fit (BM3S in Table 4) employing the data of *Saxena et al.* [1999] but not *Fiquet et al.* [2000]. Data shown include *Wang et al.* [1994], *Kato et al.* [1995], *Utsumi et al.* [1995], *Funamori et al.* [1996], *Fiquet et al.* [1998], *Saxena et al.* [1999], *Fiquet et al.* [2000], and *Li and Zhang* [2005], and *Vanpeteghem et al.* [2006].

Table 3. $MgSiO_3$ Transition Energies[a]

Transformation	ΔE_{tr} (J/kg)	References
Oxide mix → melt	1,952,455	1
Glass → Pv	680,000	2, 3
Glass → Melt	1,862,455	1, 2
En → Pv	1,100,000	3
En → PPv	1,189,000	3, 4
En → Melt	2,192,455	1
Pv +Mj → Pv	$-682{,}000 \times X_{Mj}$	5
Pv+Mj → PPv	$189{,}000-682{,}000 \times X_{Mj}$	4, 5

[a]X_{Mj} is the mole fraction of majorite. References: 1, *Ghiorso and Sack* [1995]; 2, *Richet and Bottinga* [1986]; 3, *Navrotsky* [1995]; 4, *Tsuchiya et al.* [2005]; 5, *Akaogi and Ito* [1999].

al., 1987], whereas for postperovskite we assume the value of $V_0 = 162.2$ Å^3 given by *Guignot et al.* [2007].

[15] Many formulations for γ have been proposed. In order to solve our equations we are restricted to those that obey the Mie-Grüneisen approximation $\gamma = \gamma(V)$. The most commonly used empirical form for γ, which assumes a simple power law dependence on volume, is

$$\gamma = \gamma_0 (V/V_0)^q, \tag{8}$$

where γ_0 is the Grüneisen parameter at ambient volume. Some recent studies [*Oganov et al.*, 2001; *Ono and Oganov*, 2005; *Guignot et al.*, 2007] have employed the Al'tshuler formulation for γ:

$$\gamma = \gamma_\infty + (\gamma_0 - \gamma_\infty)(V/V_0)^\beta, \tag{9}$$

where γ_∞ is the value of the Grüneisen parameter at infinite compression. This equation accounts for a decrease in the rate of change of γ with compression, a phenomenon suggested by molecular dynamic simulations. This possibility has also been modeled using other equations [e.g., *Jeanloz*, 1989; *Stixrude and Lithgow-Bertelloni*, 2005].

[16] The volume dependence of the Debye temperature is related to γ via:

$$\gamma = -\frac{d\ln\theta}{d\ln V}, \tag{10}$$

and if the form for γ given by equation (8) is assumed, this can be evaluated through integration as [*Luo et al.*, 2004]:

$$\theta = \theta_o \exp\left\{\frac{\gamma_o - \gamma}{q}\right\}. \tag{11}$$

The shock data are treated concurrently with the static data by fitting theoretical Hugoniots. For this purpose we use either equation (2) or (3) above coupled to equations (6–9) given by *Mosenfelder et al.* [2007], taking into account corrections for the porosity of the starting material [*Zel'dovich and Raizer*, 1966] and the energy of transition (ΔE_{tr}) to the postulated high-pressure phase. ΔE_{tr} is closely approximated as the difference in enthalpy of formation between the starting material and candidate high-pressure phase, taken from calorimetric data except in the case of postperovskite (Table 3).

[17] In our global fits to both static and shock data, we seek to simultaneously minimize the differences between calculated and measured values of pressure, volume, and temperature, weighted by their uncertainties (ignoring the temperature variable in the case of shock data for which it was not measured). Specifically, we fit each experimental datum (P_i, V_i, T_i) with uncertainties (σ^P_i, σ^V_i, σ^T_i) by searching for the values of V_{model} and T_{model} along the candidate equation of state surface $P_{model}(V_{model}, T_{model})$ that minimize the value of a reduced chi square statistic ($\sum_{i=1}^{n} \chi_i^2/[n-p]$), where n is the number of data points and p is the number of fit parameters). The χ^2 statistic is defined here as:

$$\chi_i^2 = \left(\frac{P_{model}(V_{model}, T_{model}) - P_i}{\sigma_i^P}\right)^2 + \left(\frac{V_{model} - V_i}{\sigma_i^V}\right)^2 + \left(\frac{T_{model} - T_i}{\sigma_i^T}\right)^2. \tag{12}$$

Reduced-χ^2 values of 1 represent the expected value for a good fit. This procedure is a significant improvement on the more straightforward approach, given that V is the independent variable in the model, of evaluating data only by errors in pressure and/or temperature relative to the model at the nominal experimental volume. Such an approach may lead to large misfits (and rejection as outliers) of data with small pressure or temperature uncertainties but large volume uncertainty.

[18] Uncertainties in all fitted parameters are determined by bootstrap estimation [*Efron*, 1982], using synthetic resamplings of the data with the number of shock and static data points independently held constant. For each trial, the reduced-χ^2 is minimized using Powell's method [*Press et al.*, 1992]. The probability distribution of the fitted parameters (standard deviations and correlations) was found to become stationary after about 400 resamplings.

[19] Our method of fitting the shock data for liquid phases varies from our approach for solids and from previous shock wave studies [*Akins et al.*, 2004; *Mosenfelder et al.*, 2007]. Thermal pressure is calculated as [cf. *Stixrude and Karki*, 2005]:

$$\Delta P_{th}(V,T) = \frac{\gamma C_v}{V}(T - T_0). \tag{13}$$

We anchor the EoS to the ambient-pressure density, sound speed, thermal expansion, enthalpy, and heat capacity for liquids at 1673 K, as determined for the bulk composition of interest from regressed partial molar properties of liquid oxides. Thus, V_0, K_{0T} (the isothermal bulk modulus), α, C_p, and ΔE_{tr} (Table 3) are fixed parameters in our models, allowing us in turn to fix K_{0S}, γ_0, and C_V at ambient pressure. Alternative models are considered using two different sets of parameters, tabulated by *Lange and Carmichael* [1990] or *Ghiorso and Kress* [2004]. Note that uncertainties on the ambient-pressure data are not taken into account in calculating final uncertainties on EoS parameters. Again, we consider both third- and fourth-order Birch-Murnaghan fits for the isentrope. In the case of $MgSiO_3$ liquid, we also take into account the available

shock temperature data [*Akins*, 2003; *Luo et al.*, 2004], using equations (10) and (11) in the work of *Mosenfelder et al.* [2007]. In fitting shock temperature data at high compression, in accord with the study of *Stixrude and Karki* [2005], we find it necessary to introduce another variable parameter, $d\ln C_V/d\ln V$, to describe the dependence of C_V on volume (note that, for simplicity, C_V is assumed to be independent of temperature at constant volume). Hence for liquid EoS fits the adjustable parameters are K'_{0S}, K''_{0S} (for fourth-order fits), q, and $(d\ln C_V/d\ln V)$.

4. Shock Wave Data

4.1. New Results and Treatment of Literature Data

[20] Results are listed in Table 2 for four new experiments on $MgSiO_3$ glass and five experiments on perovskite + majorite starting material. In our modeling, we combine our results with previous EoS data obtained using both shock wave and static compression techniques. The static data are discussed in section 5. For shock data, in addition to our new experiments we consider previous experiments on the following starting materials: $MgSiO_3$ enstatite aggregates of variable porosity (ρ_0 = 2.76–3.04 Mg/m^3) [*Simakov and Trunin*, 1973; *Marsh*, 1980]; ultraporous, equimolar mixtures of MgO and SiO_2 (ρ_0 = 1.56 Mg/m^3) [*Marsh*, 1980]; fully dense enstatite single crystals (ρ_0 = 3.20 Mg/m^3); and $MgSiO_3$ glass (ρ_0 = 2.73 Mg/m^3) [*Akins*, 2003; *Akins et al.*, 2004; *Luo et al.*, 2004]. Experiments on Fe-bearing enstatite [*Gong et al.*, 2004, and references therein] are not used in the present analysis. Figure 3 shows a comparison of all the shock wave EoS data available in the $MgSiO_3$ system. Note that the volume for each data point in this graph is normalized to the volume of the starting material of the experiment, for the sake of clarity in separating the data. Table 2 lists the parameters of all shock experiments incorporated into our thermodynamic modeling; some lower-pressure experiments shown in Figure 3 are not included as these experiments failed to reach the high-pressure phase regimes of interest (section 4.2). These data are also compared in Figure 4 in $U_s - u_p$ space. Note that shock temperature was only directly measured in the study of *Luo et al.* [2004] and in one experiment from *Akins* [2003]. In other cases, it can be estimated using equations (10) and (11) in the work of *Mosenfelder et al.* [2007].

[21] Uncertainties were not provided in the study of *Simakov and Trunin* [1973] or the tabulated shock data of *Marsh* [1980], so we arbitrarily assign uncertainties of ±1 GPa and ±1% in density to the reported values for the purposes of global fitting. For the data of *Akins* [2003], *Akins et al.* [2004], and *Luo et al.* [2004], uncertainties on shock state parameters were reevaluated to obtain new values from the given errors in measured properties, using the same analytical error propagation as used for the new experiments. Furthermore, on the basis of optical observation of remnant starting material, the wide range in densities reported for enstatite in these experiments probably reflects contributions from variable amounts of weathering material on crystal surfaces and optically visible quartz inclusions [*Zoysa*, 1985]. However, the targets were designed such that the measured shock wave traversed clear, inclusion-free portions of the crystals [*Akins*, 2003]. Accordingly, we remeasured densities on four remaining enstatite crystals that showed the least amount of these features, obtaining a well constrained value for ρ_0 of 3.199 ± 0.009 Mg/m^3 that was used to recalculate the shock parameters.

4.2. Interpreted Hugoniot Phase Regimes

[22] Phase transformations are inferred to occur during shock loading but changes in crystal structure are not observed directly in the types of experiments considered here. Interpretation of the shock wave data therefore depends on comparison to model calculations for proposed high-pressure phases and observation of slope changes along Hugoniots.

[23] Our methodology for calculating theoretical Hugoniots is described fully in section 3 and in the work of *Mosenfelder et al.* [2007]. For exploratory purposes we conduct forward modeling using EoS parameters from static experiments. Ultimately, we fit the data together with static results to refine the EoS parameters for each phase, after the most likely phase state of each point on the Hugoniot has been determined. If the EoS of the different phases are not sufficiently well separated then this exercise is circular. In the present case, however, both the a priori and a posteriori assignment of each experiment to a given phase is significant to at least 90% confidence. That is, for every experiment, the difference in quality of fit between the best phase assignment and the other possibilities, expressed as a χ^2 value (equation (12)), is at least unity.

[24] We define three phase regimes corresponding to perovskite, postperovskite, and melt. This interpretation builds on that of *Akins et al.* [2004], who assigned a sequential series of regimes with increasing pressure to the Hugoniot data in the $MgSiO_3$ system. As our interest here is in high-pressure phases in the lower mantle, we discard the data corresponding to mixed phase regimes and/or lower pressure phases (enstatite, majorite, and akimotoite). The interpreted phase regime for each data point is listed in Table 2.

[25] First, consider the new experiments on perovskite + majorite samples. The data follow a roughly linear trend in $U_s - u_p$ (Figure 4) with the exception of the highest pressure point, which is noticeably offset from the other data. Because the samples had different densities (and hence different calculated amounts of majorite), a single Hugoniot EoS ($U_s = C_0 + su_p$) cannot be fit meaningfully to the first four points, from 104 to 187 GPa. We interpret the data in this pressure range to be in the perovskite regime, while the highest-pressure experiment at 245 GPa (Shot 369) is in the postperovskite regime. Even though the pressures of three of the perovskite regime experiments are well within the postperovskite stability field, the kinetics of the phase transformation are likely inhibited due to the relatively cold temperatures reached on the Hugoniot for this dense starting material. To illustrate this point, note that at roughly comparable pressures, calculated shock temperatures in these experiments are 1500–2000 K lower than in experiments conducted using enstatite starting material.

[26] Our interpretation of the principal enstatite Hugoniot follows *Akins et al.* [2004] and *Luo et al.* [2004], with one major exception. Whereas enstatite single crystals shocked to pressures between 110 and 170 GPa were previously interpreted as having converted to perovskite, newly published, high-precision thermal EoS data on postperovskite from *Guignot et al.* [2007] lead us to separate the data into

two regimes, perovskite from 110 to 120 GPa and postperovskite from 140 to 170 GPa (with a gap in data between 120 and 140 GPa). This assignment is consistent with proposed equilibrium curves for the perovskite to postperovskite transformation [*Hirose*, 2006]. We also include the datum at 182 GPa from *Luo et al.* [2004] (shot 342) in the postperovskite regime even though enstatite shocked by *Akins et al.* [2004] to pressures between 174 and 204 GPa is assigned to a melt phase regime. This discrepancy may be attributed to nonequilibrium effects near the melting point at low degrees of superheating [*Luo et al.*, 2003] or perhaps differences in starting material. Note that if we discard shot 342 from our analysis, it has no significant effect on our global EoS fits.

[27] Shock data on $MgSiO_3$ glass were previously divided into two regimes, perovskite and melt, even though the change in slope of the Hugoniot across the proposed transition is small, indicating a small volume change upon melting. The interpretation was based on shock temperature measurements showing a significant drop in measured T_H at 120 GPa, compared to calculated Hugoniot temperatures for $MgSiO_3$ glass assuming a solid phase Hugoniot [*Luo et al.*, 2004]. Our new data extend to higher pressure (160 versus 121 GPa) in the melt regime, thereby providing better constraints on the EoS of the melt. The data scatter in the melt regime is higher than for other starting materials, possibly as a result of slight differences (for instance in fictive temperature due to different quench rates) in the glass samples used for the experiments. Nevertheless, we are able to fit all the data from 100 to 160 GPa to a liquid EoS.

[28] *Simakov and Trunin* [1973] reported limited data on porous $MgSiO_3$ enstatite samples with nominal ρ_0 = 3.04 Mg/m^3. We assign two of their data points, at 90 and 108 GPa, to perovskite, while their highest-pressure experiment at 230 GPa is clearly in the melt regime according to model calculations. *Marsh* [1980] tabulated a large number of shock data from experiments at Los Alamos National Laboratory on samples of porous enstatite with densities ranging from 2.71 to 3.01 Mg/m^3, binning the results by average ρ_0. Most of the data can be assigned to mixed-phase or low-pressure phase regimes, but 12 of the experiments from 71 to 104 GPa can be attributed to perovskite. Note that two shots on materials with initial density of ~3.01 Mg/m^3 (at Hugoniot pressures of 91 and 105 GPa; Figure 3) are not used in our analysis because these data are unacceptable outliers (they overlap with the data of initial density 2.83 Mg/m^3, with no conceivable phase transition in this range). Furthermore, one data series presented by *Marsh* [1980], with an average density of 2.71 Mg/m^3, is not used because it cannot be reconciled with any other data set, suggesting some large, systematic error in that portion of the study; in any case, most of that data is likely to be in low-pressure and/or mixed-phase regimes due to the low peak Hugoniot pressures of the experiments (between 26 and 61 GPa).

[29] Finally, we include two data points in the melt regime from experiments on very porous (ρ_0 = 1.56 Mg/m^3), equimolar mixtures of MgO and SiO_2 [*Marsh*, 1980]. The interpretation of these data follows that of *Akins et al.* [2004], with a decrease in density of about 10% attending melting on the Hugoniot at these pressures. The sample shocked to about 31 GPa, previously interpreted to have transformed to perovskite, cannot be fit to this regime, suggesting that it incompletely transformed to the high-pressure phase at the modest pressure overstep of the experiment.

5. Static *P-V-T* Data

5.1. $MgSiO_3$ Perovskite

[30] The preponderance of static compression studies on $MgSiO_3$ perovskite, conducted using different techniques with uncertain compatibility, makes it difficult to objectively select data for global inversion. Discrimination of static *P-V-T* data due to technical issues with individual studies has been discussed by previous authors attempting to fit multiple data sets [*Bina*, 1995; *Funamori et al.*, 1996; *Hama and Suito*, 1998; *Shim and Duffy*, 2000], and our selection of data is generally in accord with those studies. A table of all of the data considered in our global inversions can be found in the auxiliary material.[1]

[31] For diamond-anvil cell compression at ambient or near-ambient temperature, we prefer the modern work of *Vanpeteghem et al.* [2006] to earlier, less precise studies [*Kudoh et al.*, 1987; *Ross and Hazen*, 1990; *Mao et al.*, 1991]. Results from two multianvil studies are completely discarded because of large uncertainties in effects of differential stress [*Wang et al.*, 1991] or *T* measurement [*Morishima et al.*, 1994], while the reconnaissance Drickamer-cell study of *Funamori and Yagi* [1993] is dismissed due to extreme uncertainties in both *P* and *T* measurement. Instead, we use the multianvil studies of *Wang et al.* [1994], *Kato et al.* [1995], *Utsumi et al.* [1995], and *Funamori et al.* [1996].

[32] In the case of the *Wang et al.* [1994] data, we have discarded the results of run 8 and the three highest temperature points from run 3B. These data are characterized by significantly higher than expected volumes compared to the rest of the study, as seen in Figure 11 of *Wang et al.* [1994]. The discrepancy between these runs and the rest of the study was previously discussed by *Hama and Suito* [1998]. On the other hand, the second (heating) cycle of run 5B in their study is characterized by slightly lower than expected volumes at equal pressure, compared to the first (cooling) cycle. Although *Bina* [1995] hypothesized that this could result from compressive stress exerted by a lower pressure phase along grain boundaries of the perovskite, we consider it more likely that the discrepancy is due to a slight, systematic overestimation of pressure during the second cycle of the run. In any case we have elected to include all of the data from run 5B in our fitting.

[33] One useful way to assess static EoS data is to examine it on an f–F plot (Figure 5; see equations (4) and (5) above), because the values for the bulk modulus and its pressure derivative(s) can be readily visualized from the intercept and slope of the data trend, respectively. For instance, at first glance the study of *Li and Zhang* [2005] is appealing because of simultaneous use of X-ray diffraction and ultrasonic measurements to constrain the EoS. However, while the bulk modulus measured in this study is in excellent agreement with the Brillouin spectroscopic study of *Sinogeikin et al.* [2004] and the compression study of *Vanpeteghem et al.* [2006], as shown in Figure 5 the volume data are quite inconsistent with other studies and

[1] Auxiliary materials are available in the HTML. doi:10.1029/2008JB005900.

Table 4. EoS Parameters for Solid Phases[a]

Phase	Perovskite	Perovskite	Postperovskite
Model[b]	BM3S	BM3F	BM3
V, Å^3	162.35	162.35	162.2
K_{0S}, GPa	254.7(7)	257.0(9)	225(2)
K'_{OS}	4.26(3)	3.88(4)	4.21(7)
γ_0	2.23(9)	2.16(10)	2.61(67)
q	1.83(17)	1.37(23)	2.1(8)
C_{vm}, J/K/g	806(31)	805(30)	1035(50)
θ_0, K	736(70)	676(93)	990(146)
Reduced χ^2	1.35	2.04	0.18

[a]Uncertainties shown in parentheses.
[b]BM3S is *Saxena et al.* [1999] study included; BM3F is *Fiquet et al.* [2000] study included.

regression of these data alone would lead to an abnormally low value for the bulk modulus (note that the volume data contribute very small uncertainties to Li and Zhang's determination of K_{0S}, which is primarily constrained by P wave velocities). Therefore we leave this data set out of our models.

[34] *P-V-T* studies in the diamond-anvil cell up to much higher pressures, essential for constraining the thermal EoS of perovskite in the lower mantle, have been conducted by *Fiquet et al.* [1998], *Saxena et al.* [1999], and *Fiquet et al.* [2000]. Data from the first two studies are in reasonable accord (Figure 5), with the exception of four extreme outliers in the study of *Fiquet et al.* [1998] that we discard from our analysis (these points, all at room temperature, can be seen scattered far from the rest of the data in Figure 5; the uncertainties of these data relative to our final fits are 3σ or greater). Unfortunately, the most recent, highest-pressure data (up to 94 GPa) from *Fiquet et al.* [2000] are difficult to reconcile with either of the other two data sets, suggesting some systematic uncertainty despite the compatibility of pressure scales between the studies. Because we have no objective criteria to prefer any of these studies, we consider two possibilities in our modeling, excluding either the *Saxena et al.* [1999] or the *Fiquet et al.* [2000] data sets [cf. *Mosenfelder et al.*, 2007].

[35] One of the most difficult problems presently facing high-pressure mineral physics is reconciliation of discrepant pressure scales used in static compression studies [e.g., *Shim and Duffy*, 2000; *Fei et al.*, 2007]. Although the issue of cross-calibration between different pressure standards has not been fully resolved, we attempted to correct literature data using the new pressure scales for Au and Pt provided by *Fei et al.* [2007], who reoptimized EoS data from previous cross-calibration studies. Unfortunately, this approach is not straightforward. In the case of studies for which the measured cell volumes of the pressure standard are not provided [e.g., *Saxena et al.*, 1999; *Fiquet et al.*, 2000], the pressures must be corrected back to a reference volume for the standard before being recalculated; this approach assumes that the EoS was correctly applied in the first place. On the other hand, for one study [*Fiquet et al.*, 1998] in which the measured cell volumes of the Pt standard were given, we were unable to reproduce the corresponding pressure values given in the paper using the EoS for Pt of *Jamieson et al.* [1982]. On the basis of this discrepancy, we decided to take the *P-V-T* data at face value rather than proceed with this alternative approach.

5.2. $MgSiO_3$ Postperovskite

[36] For the EoS of postperovskite, we rely on the recent, high-precision static *P-V-T* data of *Guignot et al.* [2007], coupled to six shock experiments at considerably higher pressures that are considered to be in the postperovskite regime (see section 4.2). A couple of room temperature, high-pressure results are also provided by *Murakami et al.* [2004] and *Oganov and Ono* [2004], but these data show significant offsets from the data of *Guignot et al.* [2007]. More recently, *Ono et al.* [2006] presented a room temperature compression curve that partially overlaps that of *Guignot et al.* [2007] if pressures are calculated using the Au scale of *Jamieson et al.* [1982]. However, their data are characterized by a large discontinuity at 140 GPa that was not explained by the authors but probably results from imprecision in pressure measurement. In any case, the addition of any of these three smaller, isothermal data sets does not significantly change our overall fit.

6. Global Inversion Results

6.1. Equation of State of $MgSiO_3$ Perovskite

[37] Table 4 lists the EoS parameters of two different models for perovskite, including either the study of *Saxena et al.* [1999] (model referred to as BM3S) or that of *Fiquet et al.* [2000] (referred to as BM3F). Note that both models include the earlier data of *Fiquet et al.* [1998]. The goodness of fit to the data is represented in Figures 6a and 6b, which show graphically how the two global inversions fail to fit each respective, excluded static data set. We obtain a significantly worse overall fit with BM3F (reduced-χ^2 = 2.04) compared to BM3S (reduced-χ^2 = 1.35). Notably, the shock data (on porous and single crystal enstatite, as well as the new data on perovskite + majorite) are not as well fit with BM3F (Figure 6b). Error plots for volume are not shown but reveal similar trends.

[38] We explored fitting with fourth-order Birch-Murnaghan isentropes, which yielded nearly identical reduced-χ^2 values and thus no justification for using the extra parameter. The BM3S value of K_{0S} = 254.7(7) GPa is within uncertainty of the currently accepted value for $MgSiO_3$ perovskite (K_{0S} = 253(3) GPa) from Brillouin and ultrasonic measurements [*Sinogeikin et al.*, 2004; *Li and Zhang*, 2005]. The value of K'_{0S} from BM3S, 4.26(3), is consistent with the range of values obtained by *Li and Zhang* [2005] for $(\partial K_S/\partial P)_T$. BM3F yields a higher value for K_{0S} and, moreover and not surprisingly, a much lower value for K'_{0S} = 3.88 that is close to the value of K'_{0S} = 3.7 obtained by *Fiquet et al.* [2000].

[39] As shown in Figure 7, both models yield higher values for γ in comparison to other studies, over most of the volume range. We also obtain relatively low values for C_{vm} and θ_0, two parameters that are fixed in most studies to the theoretical Dulong- Petit limit of 3nR and the value inferred from calorimetry [*Akaogi and Ito*, 1993] of ~1000 K, respectively. Because the parameters γ and C_{vm} appear only as the product $\gamma\ C_{vm}$ in expressions for thermal pressure (e.g., equation (6) above), static compression experiments cannot separately determine these parameters. On the other hand, shock data consisting of multiple Hugoniot states (from different starting materials or porosities) are sensitive to γ alone, whereas shock temperature data constrain the C_v

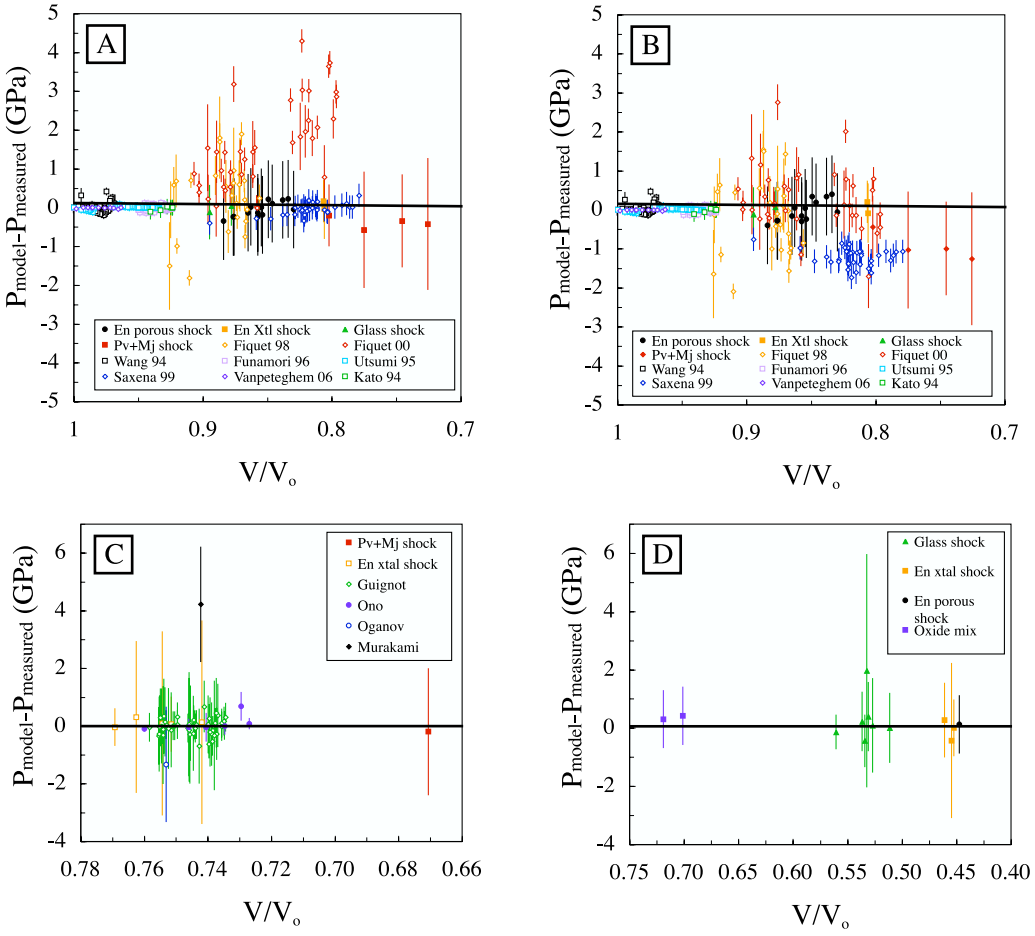

Figure 6. Differences between calculated and measured pressures as a function of volume for static and shock data, for selected EoS models from Tables 4 and 5. (a) Perovskite (BM3S model). (b) Perovskite (BM3F model). (c) Postperovskite. Data of *Ono et al.* [2006] plotted using values from Au pressure scale of *Jamieson et al.* [1982]. (d) $MgSiO_3$ liquid (BM4LC model).

function separately. The relatively large separation in pressure between the Hugoniot data, with known internal energy differences, requires the rather large value of γ within the volume range of the data. This is most true at the high-volume end of the shock data range, dictating a large q, which in turn extrapolates to a surprisingly high γ_o. In combination with the high-temperature static data, large γ_o implies relatively low values of C_v. Finally, although the fitted value of θ_0 is surprisingly low, recall from equations (10) and (11) that γ also expresses the volume dependence of θ. This means that the large values of γ, particularly the low-pressure value γ_0, in our model result in $\theta(V)$ values closer to those expected range within the volume range where perovskite is stable.

[40] Our global inversions appear well constrained, but the discrepancies among the most recent and nominally most precise *P-V-T* data point out the need for further study as in situ synchrotron-based diamond anvil cell techniques continue to improve. In particular, a new high-pressure study using the MgO pressure standard would be useful to distinguish between the discrepant static data sets and compare on the same scale to recently acquired data for the post-perovskite phase [*Guignot et al.*, 2007].

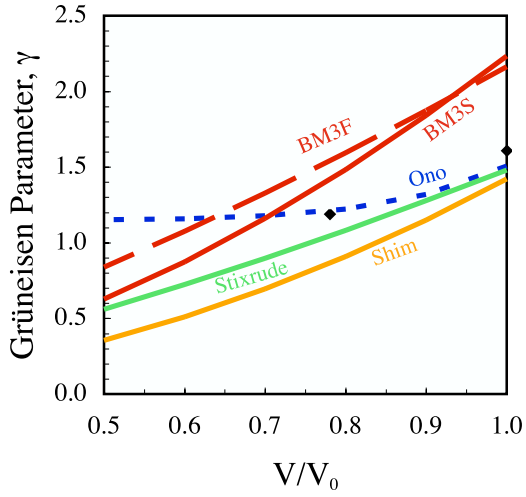

Figure 7. Grüneisen parameter of perovskite as a function of volume. Curves labeled for BM3F and BM3S models (this study, see Table 4), *Ono and Oganov* [2005], *Stixrude and Lithgow-Bertelloni* [2005], and LPT + FI + SA model from *Shim and Duffy* [2000]. Black diamonds are model results from *Tsuchiya et al.* [2005].

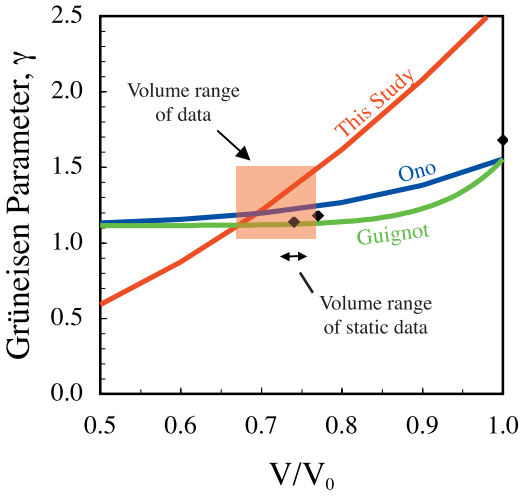

Figure 8. Grüneisen parameter of postperovskite as a function of volume. Curves labeled for this study (see Table 4), *Ono and Oganov* [2005], and *Guignot et al.* [2007]. Black diamonds are values given by *Tsuchiya et al.* [2005]. Shaded box represents volume range of all shock and static data used in fitting; volume range of static data alone shown by the double-headed arrow.

6.2. Equation of State of $MgSiO_3$ Postperovskite

[41] The shock and static data can be fit together using a third-order Birch-Murnaghan isentrope for P_s, with V_0 fixed to 162.2 Å^3 [*Guignot et al.*, 2007]. We obtain K_{0S} = 225(2) GPa and K'_{0S} = 4.21(7), values that are significantly different from the second-order Birch-Murnaghan fit (K_{0S} = 231 GPa, K' fixed to 4) that *Guignot et al.* [2007] applied to their data. As for the case of perovskite, a fourth-order fit is not justified by the data. Figure 6c shows that our model fits pressures for all of the data used in the inversion, within uncertainties. Similar goodness-of-fit applies for volumes and temperatures as well, with an overall reduced-χ^2 value of 0.18 (Table 4). We thus feel confident that the EoS of postperovskite is, perhaps surprisingly, established with significantly better confidence than that of perovskite, even though the nominal uncertainty in the parameters is higher than for either of our two model fits for perovskite.

[42] The form for γ described by our model (Figure 8) is quite different from the theoretically derived equation (equation (9)) of *Ono and Oganov* [2005] and the parameterization of *Guignot et al.* [2007], who used the same equation and assumed values for γ_0 and γ_∞, deriving the pressure dependence from a fit to their data. However, within the volume range of all of the shock and static data, there is reasonable agreement, with our values up to 20% higher than the other models. Extrapolation to higher volumes is essentially meaningless because of the high-pressure stability field (>∼ 120 GPa) of postperovskite. On the other hand, extrapolation to lower volumes outside the range of the data, which could be relevant to processes occurring in "Super Earth"-like planets, should be regarded with caution.

6.3. Equation of State of $MgSiO_3$ Liquid

[43] Consideration of all the shock data, on materials of widely varying porosity, provides constraints on the EoS for $MgSiO_3$ melt over a very wide range of pressures. Notably, our new results on $MgSiO_3$ glass extend the pressure range of its Hugoniot farther into the melt regime than previous studies, providing us with tighter constraints for obtaining the Grüneisen parameter of the melt. Furthermore, for the first time we consider the shock datum at 230 GPa from *Simakov and Trunin* [1973] in modeling the $MgSiO_3$ liquid EoS.

[44] Our method of fitting the data (section 3) allows us to derive a single EoS for the liquid from 0 to 230 GPa. This represents a significant improvement over the approach of previous high-pressure liquid EoS fits that assumed no connection between low- and high-pressure regimes [*Akins et al.*, 2004; *Mosenfelder et al.*, 2007], resulting in a large mismatch between two different EoS. Our approach assumes that there are no discontinuities in structure or thermodynamic properties with compression. This view is in accord with newer molecular dynamics simulations [*Stixrude and Karki*, 2005; *de Koker et al.*, 2008] but not with more complicated models for molecular speciation in liquids such as that of *Ghiorso* [2004].

[45] We present two inversions, using either the 1 atm properties of *Lange and Carmichael* [1990] or *Ghiorso and Kress* [2004] (designated as models BM4LC and BM4GK, respectively; Table 5). We find that an adequate fit to the melt regime data requires a fourth-order Birch-Murnaghan form for the isentrope centered at 1673 K; attempts to fit the shock data using a third-order Birch-Murnaghan isentrope while keeping ambient properties fixed yielded unacceptably large (>10) reduced-χ^2 values. Furthermore, fitting the isentrope to a Vinet EoS [*Vinet et al.*, 1987] resulted in similar reduced-χ^2 compared to the third-order Birch-Murnaghan fit. The quality of the BM4LC fit is shown in Figure 6d. Although there is a significant difference in reduced-χ^2 between BM4LC and BM4GK, we have no objective criterion to prefer either model to the other. The 1 atm properties of $MgSiO_3$ liquid were defined indirectly by both *Lange and Carmichael* [1990] and *Ghiorso and Kress* [2004] from the partial molar properties of MgO and SiO_2, regressed to measurements on a large number of liquids but nevertheless poorly constrained compared to other compositions that have been more directly measured. Note that both models give overlapping values, within uncertainty, for K'_{0S} and q.

[46] Our best fitting functions for γ describe a substantial

Table 5. EoS Fit Parameters for Melts[a]

Melt Composition	$MgSiO_3$	$MgSiO_3$	Mg_2SiO_4	Mg_2SiO_4
Model[b]	BM4LC	BM4GK	BM4LC	BM4GK
V, m^3/kg ± × 10^{-5})	38.202	38.575	35.397	36.065
K_{0S}, GPa	24.7	20.8	41.0	25.1
K'_{0S}	9.2(5)	10.2(7)	4.36(3)	6.62(1)
K''_{0S}, GPa^{-1}	−1.87(27)	−2.86(48)	−0.068(3)	−0.059(5)
γ_0	0.37	0.46	0.63	0.63
q	−1.71(31)	−1.35(39)	−2.066(4)	−2.025(1)
C_v, J/K/g	1691	1635	1733	1689
$dlnC_v/dlnV$	1.31(30)	1.12(0.16)	na[c]	na[c]
Reduced χ^2	1.89	2.79	10^{-4}	10^{-5}

[a]Uncertainties shown in parentheses. No uncertainties shown for fixed 1 atm/1673 K properties.
[b]Data source for 1 atm (= 10^5 × 1.01325 N/m^2) parameters. LC is *Lange and Carmichael* [1990]; GC is *Ghiorso and Kress* [2004].
[c]Unconstrained; see text for explanation.

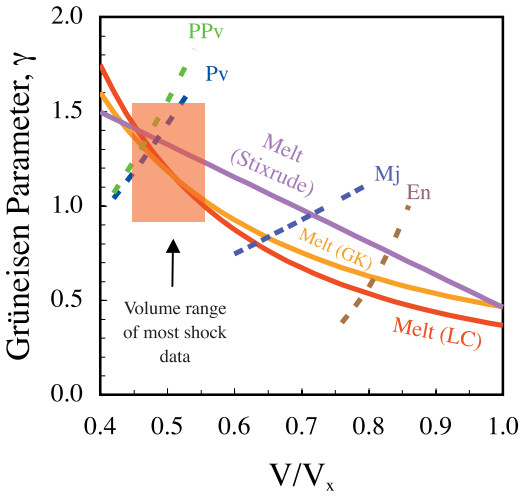

Figure 9. Grüneisen parameter of $MgSiO_3$ liquid as a function of volume referenced to V_x, the volume of the liquid at 1 atm (= $10^5 \times 1.01325$ N/m^2) and 1673 K [*Lange and Carmichael*, 1990]. Labeled curves for the liquid include our two models, BM4LC and BM4GK (see Table 5) and model of *Stixrude and Karki* [2005]. Also shown are γ functions for postperovskite (this study), and perovskite (this study, BM3S model), majorite, and enstatite [*Stixrude and Lithgow-Bertelloni*, 2005]. Shaded box shows volume range for all of shock data except the two points from *Marsh* [1980], which lie near $V/V_x = 0.7$.

increase in this parameter with compression. As with our previous work in the Mg_2SiO_4 system [*Mosenfelder et al.*, 2007], we thus confirm once again the theoretical prediction of *Stixrude and Karki* [2005] that the behavior of γ upon compression in silicate liquids is the reverse of that in solids. Figure 9 shows a comparison of our functions for γ with that of *Stixrude and Karki* [2005], illustrating a remarkable correspondence between our studies at high values of compression (near $V/V_x = 0.5$, which is within the range of the shock data). Differences are mostly attributable to our adoption of a power law volume dependence, whereas *Stixrude and Karki* [2005] fit a linear volume dependence to their model results. As interpreted by *Stixrude and Karki* [2005], the increase in γ with compression could reflect the steady increase with compression of Si coordination number, taking on the character of solid phases with higher-coordinated Si and higher γ. We follow *Stixrude and Karki* [2005] in showing this phenomenon graphically in Figure 9, by plotting γ functions for solid $MgSiO_3$ phases with increasing Si coordination relative to the liquid phase (note that the transition from perovskite to postperovskite does not involve a Si coordination change).

[47] Finally, we note that our fitted values of $d\ln C_V/d\ln V$, a parameter introduced in order to fit the shock temperature data of *Luo et al.* [2004], are high in comparison to the volume dependence derived by *Stixrude and Karki* [2005]. Furthermore, the decrease in C_V with pressure that appears to be justified by both of our studies is in contrast to the apparent case for SiO_2 liquid, in which C_V initially rises steeply above 3nR according to shock temperature measurements [*Hicks et al.*, 2006]. Additional precise shock temperature measurements [e.g., *Spaulding et al.*, 2007] clearly would be useful to resolve these apparent discrepancies, but importantly we note that if the shock temperature data are not used in the fitting the only significant impact is that $d\ln C_V/d\ln V$ is not constrained; we obtain similar values for all other parameters, including q.

6.4. Revised Equation of State of Mg_2SiO_4 Liquid

[48] In a previous study [*Mosenfelder et al.*, 2007], we fit shock data on Mg_2SiO_4 forsterite and wadsleyite using a third-order Birch-Murnaghan form to determine the EoS of liquid of the same composition at very high pressures. As evident from Figure 7 of *Mosenfelder et al.* [2007], the high-pressure EoS shows a large mismatch with an EoS calculated by extrapolating melt properties at ambient pressure. Here we refit the data using the same approach as for $MgSiO_3$, in order to derive a single EoS from 1 atm to 200 GPa that is anchored to ambient pressure data. The parameters of our new fits are given in Table 5. Again, we find that using a fourth-order B-M isentrope substantially improves the fits. Our new values for q describe γ functions that are still significantly different from that derived by the more recent molecular dynamics study of *de Koker et al.* [2008] (whose EoS model only fits our highest-pressure shock data for wadsleyite), although both models share the key behavior of γ increasing upon compression. It seems clear that both more shock data and further molecular dynamics study, perhaps with larger cells to account for the larger formula unit of Mg_2SiO_4 (compared to $MgSiO_3$), will be needed to resolve this discrepancy and confidently pin down the volume dependence of γ for this liquid. Accordingly, we consider different models for the EoS of Mg_2SiO_4 liquid when considering applications below in sections 7.2 and 7.3.

7. Implications

7.1. Thermal Expansion and Convection in the Mantle

[49] The coefficient of thermal expansion, $\alpha = 1/V(\partial V/\partial T)_P$, is an important factor in the Rayleigh number, which governs the vigor of convection. It is also commonly used to constrain the chemical composition of the mantle [e.g., *Wang et al.*, 1994; *Fiquet et al.*, 1998]. Although we have not chosen to use α as a fit parameter in our modeling, it can be calculated from our fit parameters, at any given volume, via the thermodynamic identity $\alpha = \gamma\rho C_V/K_T$. To illustrate this aspect of the EoS of perovskite and postperovskite, we plot α for these phases as a function of pressure in Figure 10, assuming a typical mantle adiabat with a potential temperature (T_p) of 1673 K. Our results suggest that thermal expansion of postperovskite is about 50% higher than that of perovskite at comparable conditions. In isolation, this suggests that the existence of postperovskite in the D″ layer of the Earth should have the effect of vigorously promoting convection. In particular, substantially less thickening of the thermal-boundary layer (at and above the CMB) should be required to initiate a plume in the postperovskite stability region compared to the layer above containing perovskite. However, this result should be interpreted with caution as other physical parameters such as viscosity and thermal diffusivity influence the vigor of convection and the effect of postperovskite on these parameters remains unknown.

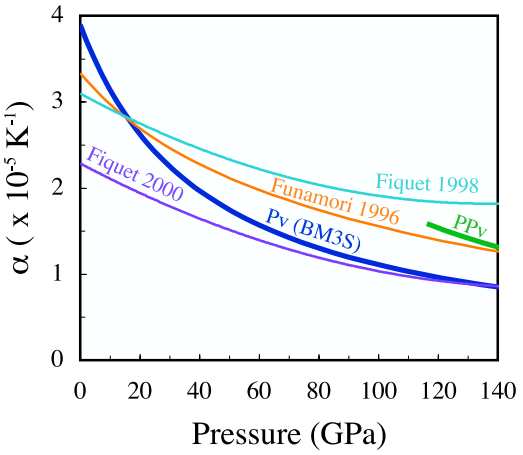

Figure 10. Thermal expansion coefficient as a function of pressure for perovskite (BM3S model) and postperovskite. Also shown are curves from the studies of *Funamori et al.* [1996], *Fiquet et al.* [1998], and *Fiquet et al.* [2000], calculated along a mantle adiabat with potential temperature of 1673 K.

[50] In Figure 10 we also show values of α calculated from the EoS of *Funamori et al.* [1996], *Fiquet et al.* [1998], and *Fiquet et al.* [2000] for comparison. Our values are within the range of previous estimates. Interestingly, our curve is closest to that of *Fiquet et al.* [2000], even though we show here the BM3S inversion that excludes their data. While the source of the discrepancy between the *P-V-T* data of *Fiquet et al.* [2000] and other studies is not known, it seems to affect their 300 K and high-temperature data equally, such that the thermal expansion is not discrepant.

[51] Although our estimate for γ is higher at most mantle pressures than other models, our fitted values of C_V are lower than the fixed values typically used by other studies and the product of these variables yields estimates of α similar to previous studies. However, the strong volume dependence of γ in our model results in a stronger pressure dependence of α compared to most other models. Consequently, our value of α for perovskite contributes to a value of the overall Rayleigh number for the lower mantle similar to previous models but implies a stronger than expected pressure dependence to the vigor of convection, with a significant minimum for α in the highest-pressure part of the perovskite stability field.

7.2. Density of Melts in the Lower Mantle

[52] At low pressures, density changes upon melting of silicates are almost ubiquitously negative. However, as proposed by *Stolper et al.* [1981] and subsequently verified by experimental studies [e.g., *Rigden et al.*, 1984; *Agee and Walker*, 1988], the densities of mafic or ultramafic liquids and coexisting solid phases cross over with increasing pressure in the upper mantle due to the higher compressibility of melts compared to solids. An analogous density crossover in the lower mantle is probably necessitated by the partial melt hypothesis for ULVZ [*Williams and Garnero*, 1996; *Lay et al.*, 2004] because the presence of significant partial melt is easier to explain if it is dynamically stable given that connectivity of even low degree partial melts is thought to be high at these conditions and, moreover, the time needed to percolate melt upward from an unstable layer is correspondingly short [e.g., *Lay et al.*, 2004].

[53] Previous shock wave studies [*Akins et al.*, 2004; *Mosenfelder et al.*, 2007] and molecular dynamic simulations [*Belonoshko and Dubrovinsky*, 1996; *Stixrude and Karki*, 2005; *Wan et al.*, 2007; *de Koker et al.*, 2008] show that the densities of solids and liquids in the $MgSiO_3$ and Mg_2SiO_4 system closely approach each other at high compression. Our refinement in this study of the EoS for liquid $MgSiO_3$ and Mg_2SiO_4 permits us to further constrain the possibility of density crossovers in the lower mantle, which we show in Figure 11. Each graph shows our model for the density of the liquid along with appropriate Fe-free mantle solids, based on our EoS for perovskite and postperovskite and literature EoS for other phases [*Stixrude and Lithgow-Bertelloni*, 2005]. Each density curve is plotted

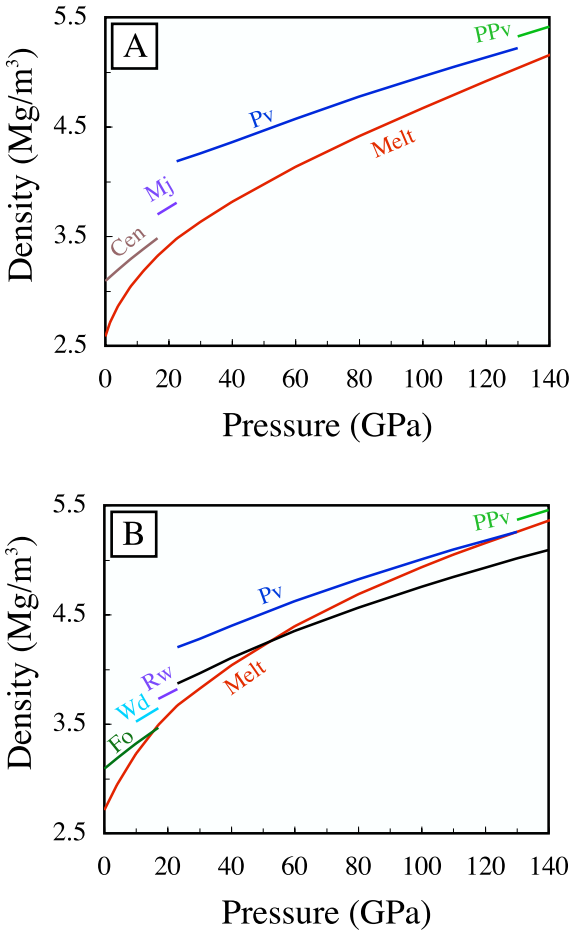

Figure 11. (a) Density of high-pressure phases evaluated along the liquidus of $MgSiO_3$. (b) Density of high-pressure phases evaluated along the liquidus of Mg_2SiO_4. Curves for clinoenstatite (Cen), majorite (Mj), wadsleyite (Wd), ringwoodite (Rw), and periclase (Pe) calculated using parameters from *Stixrude and Lithgow-Bertelloni* [2005]. Curve for perovskite (Pv) shown for BM3S model; BM3F model for perovskite nearly overlaps on these graphs. Curves for postperovskite (PPv) and liquids from this study (see Tables 4 and 5).

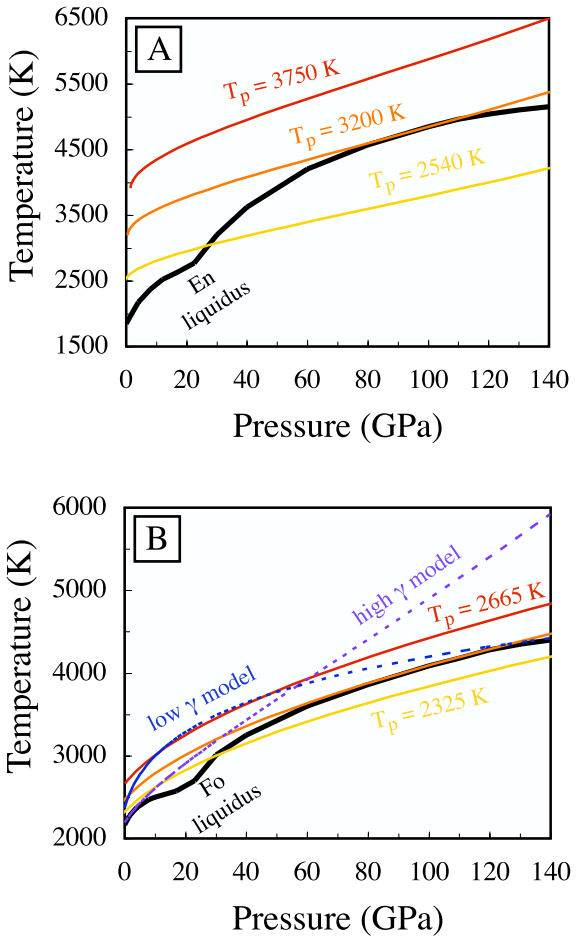

Figure 12. Comparison of liquidus curves (thick solid curves) with representative isentropic temperature profiles (thin curves) during cooling of a deep magma ocean. (a) $MgSiO_3$ composition. (b) Mg_2SiO_4 composition, showing three adiabats (thin solid curves) corresponding to model using EoS parameters from *de Koker et al.* [2008], and two adiabats from our previous study [*Mosenfelder et al.*, 2007] corresponding to our model ("high γ") and that of *Miller et al.* [1991]("low γ").

along the liquidus of the appropriate composition rather than along an isentrope or isotherm [cf. *Agee and Walker*, 1988]. The liquidus curves (shown explicitly in Figure 12) are from *Presnall* [1995] for the upper mantle, while for the lower mantle the curves are based on *Luo et al.* [2004], modified to account for the revised assignment of shock temperature data and of liquid/solid density crossovers in this work.

[54] For $MgSiO_3$, we concur with theoretical studies [*Stixrude and Karki*, 2005; *Wan et al.*, 2007] that density crossovers in the end-member system do not occur until pressures higher than that of the CMB are reached (Figure 11a). Our revised model for Mg_2SiO_4 (Figure 11b) also shows that a crossover of this liquid with perovskite does not occur until ~130 GPa (the crossover with a pyrolite-composition perovskite + periclase assemblage would be at somewhat lower pressure), whereas previously we showed a crossover close to 100 GPa. Nevertheless, the effects of Fe and other elements (Ca, Al) on the densities of real lower mantle liquids are likely to result in density inversion near the CMB if these elements partition preferentially into the melt, as pointed out by previous authors [*Stixrude and Karki*, 2005; *Wan et al.*, 2007].

7.3. Magma Ocean Thermal Evolution

[55] The dynamics and crystallization behavior of a vigorously convecting (and thus nearly adiabatic) magma ocean are fundamentally affected by its temperature profile, which is effectively equal to the Grüneisen parameter of the magma through the simple thermodynamic identity $\gamma = (\partial \ln T/\partial \ln \rho)_S$ [*Miller et al.*, 1991]. Our previous work documenting the increase in γ with compression for Mg_2SiO_4 liquid led us to speculate that cooling of a deep magma ocean (i.e., after the postulated moon-forming impact) could result in crystallization from the top down (or near the top, at pressures corresponding to the modern-day transition zone), as opposed to the conventional view that differentiation occurs by fractionation of perovskite at the bottom of the ocean [e.g., *Miller et al.*, 1991; *Solomatov*, 2007]. Our new data on $MgSiO_3$ and reanalysis of the Mg_2SiO_4 shock data allow us to further evaluate this possibility.

[56] Figures 12a and 12b show representative adiabats for $MgSiO_3$ and Mg_2SiO_4 compositions, compared to liquidi estimated as outlined in section 7.2. In each case we show one adiabat above the liquidus, one adiabat representing the temperature profile at the onset of first crystallization, and one adiabat corresponding to nearly complete crystallization. For $MgSiO_3$ liquid, we show adiabats corresponding to EoS parameters from our BM4LC inversion. According to this simple model, the first crystals form when an adiabat with a potential temperature (T_p) of 3200 K becomes tangent to the liquidus in the middle of the lower mantle, at a pressure of ~80 GPa; thus differentiation begins in the middle of the mantle rather than the bottom.

[57] For Mg_2SiO_4 we show several alternatives (Figure 12b): the conventional estimate of $q = 1$ for liquids ("low gamma model," dashed curve), our previous estimate based on shock data ("high gamma" model, dashed curve), and an alternative model (three solid curves) based on the formulation for γ provided by *de Koker et al.* [2008]. In this latter case we also use their formulation for C_V but our fourth-order EoS parameters for the bulk modulus. This model shows behavior analogous to that in the $MgSiO_3$ system, with the first crystals forming upon intersection of an adiabat with the liquidus in the midmantle. Thus, despite uncertainties in the EoS of the liquid (as well as the *P-T* profile of the liquidus), the conclusion appears to be robust that the increase in γ with compression that is now documented for silicate liquids has important effects on crystallization behavior that should be considered in future models of magma ocean evolution. *Labrosse et al.* [2007] have already explored this possibility with an intriguing model for a slowly cooling basal melt layer that in its present-day manifestation as a basal melt layer, represents a critical "hidden reservoir" for much of the Earth's geochemical budget. Whether there are broader consequences of the relations we illustrate between adiabats and liquidus curves depends to a large extent on the style of magma ocean differentiation, specifically whether or not early perovskite

crystallization is accompanied by settling and fractionation [*Solomatov*, 2007]. If the rheological transition to solid-like (mush) convection that occurs near 60% crystal fraction is a critical event in magma ocean evolution [*Solomatov*, 2007], the models for γ presented in this work predict that the bulk of the lower mantle will experience this transition over a rather small interval of potential temperature.

[58] **Acknowledgments.** Funding for this work was provided by the Bayerisches Geoinstitut and by National Science Foundation grant EAR-0207934. We thank H. Fischer for technical support of multianvil experiments in Germany; M. Long, P. Gelle, and R. Oliver for support with the shock wave experiments at Caltech; B. Balta for obtaining microprobe analyses; and T. Schneider for advice on statistics.

References

Agee, C. B., and D. Walker (1988), Static compression and olivine flotation in ultrabasic silicate liquid, *J. Geophys. Res.*, *93*, 3437–3449, doi:10.1029/JB093iB04p03437.

Akaogi, M., and E. Ito (1993), Heat capacity of $MgSiO_3$ perovskite, *Geophys. Res. Lett.*, *20*, 105–108, doi:10.1029/92GL02655.

Akaogi, M., and E. Ito (1999), Calorimetric study on majorite-perovskite transition in the system $Mg_4Si_4O_{12}$-$Mg_3Al_2Si_3O_{12}$: Transition boundaries with positive pressure-temperature slopes, *Phys. Earth Planet. Inter.*, *114*, 129–140, doi:10.1016/S0031-9201(99)00039-4.

Akins, J. A. (2003), Dynamic compression of minerals in the MgO-FeO-SiO_2 system, Ph.D. thesis, Calif. Inst. of Technol., Pasadena, Calif.

Akins, J. A., S.-N. Luo, P. D. Asimow, and T. J. Ahrens (2004), Shock-induced melting of $MgSiO_3$ perovskite and implications for melts in Earth's lowermost mantle, *Geophys. Res. Lett.*, *31*, L14612, doi:10.1029/2004GL020237.

Anderson, O. L. (1995), *Equations of State of Solids for Geophysicists and Ceramic Science*, 405 pp., Oxford Univ. Press, New York.

Belonoshko, A. B., and L. S. Dubrovinsky (1996), Molecular and lattice dynamics study of the MgO-SiO_2 system using a transferable interatomic potential, *Geochim. Cosmochim. Acta*, *60*, 1645–1656, doi:10.1016/0016-7037(96)00053-1.

Bina, C. R. (1995), Confidence limits for silicate perovskite equations of state, *Phys. Chem. Miner.*, *22*, 375–382, doi:10.1007/BF00213334.

de Koker, N. P., L. Stixrude, and B. B. Karki (2008), Thermodynamics, structure, dynamics, and melting of Mg_2SiO_4 liquid at high pressure, *Geochim. Cosmochim. Acta*, *72*, 1427–1441, doi:10.1016/j.gca.2007.12.019.

Durben, D. J., and G. H. Wolf (1992), High-temperature behavior of metastable $MgSiO_3$ perovskite: A Raman spectroscopic study, *Am. Mineral.*, *77*, 890–893.

Efron, B. (1982), *The Jackknife, the Bootstrap, and Other Resampling Plans*, 92 pp., Soc. for Ind. and Appl. Math., Philadelphia, Pa.

Fei, Y., A. Ricolleau, M. Frank, K. Mibe, G. Shen, and V. Prakapenka (2007), Toward an internally consistent pressure scale, *Proc. Natl. Acad. Sci. U. S. A.*, *104*, doi:10.1073/pnas.0609013104.

Fiquet, G., D. Andrault, A. Dewaele, T. Charpin, M. Kunz, and D. Haüsermann (1998), P-V-T equation of state of MgSiO3 perovskite, *Phys. Earth Planet. Inter.*, *105*, 21–31, doi:10.1016/S0031-9201(97)00077-0.

Fiquet, G., A. Dewaele, D. Andrault, M. Kunz, and T. Le Bihan (2000), Thermoelastic properties and crystal structure of $MgSiO_3$ perovskite at lower mantle pressure and temperature conditions, *Geophys. Res. Lett.*, *27*, 21–24, doi:10.1029/1999GL008397.

Frost, D. J., B. T. Poe, R. G. Trønnes, C. Liebske, A. Duba, and D. C. Rubie (2004), A new large-volume multianvil system, *Phys. Earth Planet. Inter.*, *143–144*, 507–514, doi:10.1016/j.pepi.2004.03.003.

Funamori, N., and T. Yagi (1993), High pressure and high temperature in situ X-ray observation of $MgSiO_3$ perovskite under lower mantle conditions, *Geophys. Res. Lett.*, *20*, 387–390, doi:10.1029/92GL02960.

Funamori, N., T. Yagi, W. Utsumi, T. Kondo, and T. Uchida (1996), Thermoelastic properties of $MgSiO_3$ perovskite determined by in situ X ray observations up to 30 GPa and 2000 K, *J. Geophys. Res.*, *101*, 8257–8269, doi:10.1029/95JB03732.

Ghiorso, M. S. (2004), An equation of state for silicate melts. III. Analysis of stoichiometric liquids at elevated pressure: Shock compression data, molecular dynamics simulations and mineral fusion curves, *Am. J. Sci.*, *304*, 752–810, doi:10.2475/ajs.304.8-9.752.

Ghiorso, M. S., and V. C. Kress (2004), An equation of state for silicate melts. II. Calibration of volumetric properties at 10^5 Pa, *Am. J. Sci.*, *304*, 679–751, doi:10.2475/ajs.304.8-9.679.

Ghiorso, M. S., and R. O. Sack (1995), Chemical mass transfer in igneous processes IV. A revised and internally consistent thermodynamic model for the interpolation and extrapolation of liquid-solid equilibria in magmatic systems at elevated temperatures and pressures, *Contrib. Mineral. Petrol.*, *119*, 197–212, doi:10.1007/BF00307281.

Gong, Z., Y. Fei, F. Dai, L. Zhang, and F. Jing (2004), Equation of state and phase stability of mantle perovskite up to 140 GPa shock pressure and its geophysical implications, *Geophys. Res. Lett.*, *31*, L04614, doi:10.1029/2003GL019132.

Guignot, N., D. Andrault, G. Morard, N. Bolfan-Casanova, and M. Mezouar (2007), Thermoelastic properties of post-perovskite phase $MgSiO_3$ determined experimentally at core-mantle boundary P-T conditions, *Earth Planet. Sci. Lett.*, *256*, 162–168, doi:10.1016/j.epsl.2007.01.025.

Gwanmesia, G. D., B. Li, and R. C. Liebermann (1993), Hot Pressing of polycrystals of high-pressure phases of mantle minerals in multi-anvil apparatus, *Pure Appl. Geophys.*, *141*, 467–484, doi:10.1007/BF00998340.

Hama, J., and K. Suito (1998), Equation of state of $MgSiO_3$ perovskite and its thermoelastic properties under lower mantle conditions, *J. Geophys. Res.*, *103*, 7443–7462, doi:10.1029/97JB03672.

Hicks, D. G., T. R. Boehly, J. H. Eggert, J. E. Miller, P. M. Celliers, and G. W. Collins (2006), Dissociation of liquid silica at high pressures and temperatures, *Phys. Rev. Lett.*, *97*, 025502, doi:10.1103/PhysRevLett.97.025502.

Hirose, K. (2006), Postperovskite phase transition and its geophysical implications, *Rev. Geophys.*, *44*, RG3001, doi:10.1029/2005RG000186.

Horiuchi, H., E. Ito, and D. Weidner (1987), Perovskite-type $MgSiO_3$: Single-crystal X-ray diffraction study, *Am. Mineral.*, *72*, 357–360.

Jackson, I., and S. M. Rigden (1996), Analysis of P-V-T data: Constraints on the thermoelastic properties of high-pressure minerals, *Phys. Earth Planet. Inter.*, *96*, 85–112, doi:10.1016/0031-9201(96)03143-3.

Jamieson, J. C., F. N. Fritz, and M. H. Manghnani (1982), Pressure measurement at high temperature in X-ray diffraction studies: Gold as a primary standard, in *High Pressure Research in Geophysics*, edited by S. Akimoto and M. H. Manghnani, pp. 27–48, D. Reidel, Boston, Mass.

Jeanloz, R. (1989), Shock wave equation of state and finite strain theory, *J. Geophys. Res.*, *94*, 5873–5886, doi:10.1029/JB094iB05p05873.

Kato, T., E. Ohtani, H. Morishima, D. Yamazaki, A. Suzuki, M. Suto, T. Kubo, T. Kikegawa, and O. Shimomura (1995), In situ X ray observation of high-pressure phase transitions of $MgSiO_3$ and thermal expansion of $MgSiO_3$ perovskite at 25 GPa by double-stage multianvil apparatus, *J. Geophys. Res.*, *100*, 20,475–20,481, doi:10.1029/95JB01688.

Kudoh, Y., E. Ito, and H. Takeda (1987), Effect of pressure on the crystal structure of perovskite-type $MgSiO_3$, *Phys. Chem. Miner.*, *14*, 350–354, doi:10.1007/BF00309809.

Labrosse, S., J. W. Hernlund, and N. Coltice (2007), A crystallizing dense magma ocean at the base of the Earth's mantle, *Nature*, *450*, 866–869, doi:10.1038/nature06355.

Lange, R. A., and I. S. E. Carmichael (1990), Thermodynamic properties of silicate liquids with an emphasis on density, thermal expansion, and compressibility, in *Modern Methods of Igneous Petrology*, edited by J. Nicholls and K. Russell, pp. 25–64, Mineral. Soc. of Am., Chantilly, Va.

Lay, T., E. J. Garnero, and Q. Williams (2004), Partial melting in a thermo-chemical boundary layer at the base of the mantle, *Phys. Earth Planet. Inter.*, *146*, 441–467, doi:10.1016/j.pepi.2004.04.004.

Li, B., and J. Zhang (2005), Pressure and temperature dependence of elastic wave velocity of MgSiO3 perovskite and the composition of the lower mantle, *Phys. Earth Planet. Inter.*, *151*, 143–154.

Litasov, K., E. Ohtani, F. Langenhorst, H. Yurimoto, T. Kubo, and T. Kondo (2003), Water solubility in Mg-perovskites and water storage capacity in the lower mantle, *Earth Planet. Sci. Lett.*, *211*, 189–203, doi:10.1016/S0012-821X(03)00200-0.

Luo, S.-N., J. L. Mosenfelder, P. D. Asimow, and T. J. Ahrens (2002), Direct shock wave loading of Stishovite to 235 GPa: Implications for perovskite stability relative to an oxide assemblage at lower mantle conditions, *Geophys. Res. Lett.*, *29*(14), 1691, doi:10.1029/2002GL015627.

Luo, S.-N., T. J. Ahrens, and P. D. Asimow (2003), Polymorphism, superheating, and amorphization of silica upon shock wave loading and release, *J. Geophys. Res.*, *108*(B9), 2421, doi:10.1029/2002JB002317.

Luo, S.-N., J. A. Akins, T. J. Ahrens, and P. D. Asimow (2004), Shock-compressed $MgSiO_3$ glass, enstatite, olivine, and quartz: Optical emission, temperatures, and melting, *J. Geophys. Res.*, *109*, B05205, doi:10.1029/2003JB002860.

Mao, H.-K., R. J. Hemley, Y. Fei, J. F. Shu, L. C. Chen, A. P. Jephcoat, Y. Wu, and W. A. Bassett (1991), Effect of pressure, temperature, and composition on lattice parameters and density of (Fe, Mg)SiO_3-perovskites to 30 GPa, *J. Geophys. Res.*, *96*, 8069–8079, doi:10.1029/91JB00176.

Marsh, S. P. (1980), *LASL Shock Hugoniot Data*, 658 pp., Univ. of Calif. Press, Berkeley.

McMillan, P., M. Akaogi, E. Ohtani, Q. Williams, R. Nieman, and R. Sato (1989), Cation disorder in garnets along the $Mg_3Al_2Si_3O_{12}$-$Mg_4Si_4O_{12}$

join: An infrared, Raman and NMR study, *Phys. Chem. Miner.*, *16*, 428–435, doi:10.1007/BF00197012.

Miller, G. H., E. M. Stolper, and T. J. Ahrens (1991), The equation of state of a molten komatiite 2. Application to komatiite petrogenesis and the Hadean mantle, *J. Geophys. Res.*, *96*, 11,849–11,864, doi:10.1029/91JB01203.

Mitchell, A. C., and W. J. Nellis (1981), Shock compression of aluminum, copper, and tantalum, *J. Appl. Phys.*, *52*, 3363–3374, doi:10.1063/1.329160.

Morishima, H., E. Ohtani, T. Kato, O. Shimomura, and T. Kikegawa (1994), Thermal expansion of $MgSiO_3$ perovskite at 20.5 GPa, *Geophys. Res. Lett.*, *21*, 899–902, doi:10.1029/94GL00844.

Mosenfelder, J. L., P. D. Asimow, and T. J. Ahrens (2007), Thermodynamic properties of Mg_2SiO_4 liquid at ultra-high pressures from shock measurements to 200 GPa on forsterite and wadsleyite, *J. Geophys. Res.*, *112*, B06208, doi:10.1029/2006JB004364.

Murakami, M., K. Hirose, K. Kawamura, N. Sata, and Y. Ohishi (2004), Post-perovskite transition in $MgSiO_3$, *Science*, *304*, 855–858, doi:10.1126/science.1095932.

Navrotsky, A. (1995), Thermodynamic properties of minerals, in *Mineral Physics and Crystallography: A Handbook of Physical Constants*, *Ref. Shelf*, vol. 2, edited by T. J. Ahrens, pp. 18–28, AGU, Washington, D. C.

Oganov, A. R., and S. Ono (2004), Theoretical and experimental evidence for a post-perovskite phase of $MgSiO_3$ in Earth's D'' layer, *Nature*, *430*, 445–448, doi:10.1038/nature02701.

Oganov, A. R., J. P. Brodholt, and G. D. Price (2001), Ab initio elasticity and thermal equation of state of $MgSiO_3$ perovskite, *Earth Planet. Sci. Lett.*, *184*, 555–560, doi:10.1016/S0012-821X(00)00363-0.

Ono, S., and A. R. Oganov (2005), In situ observations of phase transition between perovskite and $CaIrO_3$-type phase in $MgSiO_3$ and pyrolitic mantle composition, *Earth Planet. Sci. Lett.*, *236*, 914–932, doi:10.1016/j.epsl.2005.06.001.

Ono, S., T. Kikegawa, and Y. Ohishi (2006), Equation of state of $CaIrO_3$-type $MgSiO_3$ up to 144 GPa, *Am. Mineral.*, *91*, 475–478, doi:10.2138/am.2006.2118.

Presnall, D. C. (1995), Phase diagrams of Earth-forming minerals, in *Mineral Physics and Crystallography: A Handbook of Physical Constants*, *Ref. Shelf*, vol. 2, edited by T. J. Ahrens, pp. 248–268, AGU, Washington, D.C.

Press, W. H., S. A. Teukolsky, W. T. Vetterling, and B. P. Flannery (1992), *Numerical Recipes in C: The Art of Scientific Computing*, 994 pp., Cambridge Univ. Press, New York.

Richet, P., and Y. Bottinga (1986), Thermochemical properties of silicate glasses and liquids: A review, *Rev. Geophys.*, *24*, 1–25, doi:10.1029/RG024i001p00001.

Rigden, S. M., T. J. Ahrens, and E. M. Stolper (1984), Densities of liquid silicates at high pressure, *Science*, *226*, 1071–1074, doi:10.1126/science.226.4678.1071.

Ross, N. L., and R. M. Hazen (1990), High-pressure crystal chemistry of $MgSiO_3$ perovskite, *Phys. Chem. Miner.*, *17*, 228–237, doi:10.1007/BF00201454.

Rubie, D. C. (1999), Characterising the sample environment in multianvil high-pressure experiments, *Phase Transit.*, *68*, 431–451, doi:10.1080/01411599908224526.

Saxena, S. K., L. S. Dubrovinksy, F. Tutti, and T. Le Bihan (1999), Equation of state of $MgSiO_3$ with the perovskite structure based on experimental measurement, *Am. Mineral.*, *84*, 226–232.

Shim, S.-H., and T. S. Duffy (2000), Constraints on the P-V-T equation of state of $MgSiO_3$ perovskite, *Am. Mineral.*, *85*, 354–363.

Sidorin, I., M. Gurnis, and D. V. Helmberger (1999), Evidence for a ubiquitous seismic discontinuity at the base of the mantle, *Science*, *286*, 1326–1331, doi:10.1126/science.286.5443.1326.

Simakov, G. V., and R. F. Trunin (1973), On the existence of overdense perovskite structures in magnesium silicates under conditions of high pressure (English translation), *Izvestiya Earth Phys.*, *9*, 603–604.

Sinogeikin, S. V., J. Zhang, and J. D. Bass (2004), Elasticity of single crystal and polycrystalline $MgSiO_3$ perovskite by Brillouin spectroscopy, *Geophys. Res. Lett.*, *31*, L06620, doi:10.1029/2004GL019559.

Solomatov, V. (2007), Magma oceans and primordial mantle differentiation, in *Evolution of the Earth*, *Treatise on Geophys.*, vol. 9, edited by D. Stevenson, pp. 91–119, Elsevier, New York.

Spaulding, D. K., D. G. Hicks, R. F. Smith, J. H. Eggert, R. S. Mcwilliams, G. W. Collins, and R. Jeanloz (2007), Temperature measurements and melting of shock-compressed minerals, *Eos Trans. AGU*, *88*(52), Fall Meet. Suppl., Abstract MR54A–03.

Stixrude, L., and B. Karki (2005), Structure and freezing of $MgSiO_3$ liquid in Earth's lower mantle, *Science*, *310*, 297–299, doi:10.1126/science.1116952.

Stixrude, L., and C. Lithgow-Bertelloni (2005), Thermodynamics of mantle minerals–I. Physical properties, *Geophys. J. Int.*, *162*, 610–632, doi:10.1111/j.1365-246X.2005.02642.x.

Stolper, E., D. Walker, B. H. Hager, and J. F. Hays (1981), Melt segregation from partially molten source regions: The importance of melt density and source region size, *J. Geophys. Res.*, *86*, 6261–6271, doi:10.1029/JB086iB07p06261.

Tsuchiya, J., T. Tsuchiya, and R. M. Wentzcovich (2005), Vibrational and thermodynamic properties of MgSiO3 postperovskite, *J. Geophys. Res.*, *110*, B02204, doi:10.1029/2004JB003409.

Utsumi, W., N. Funamori, T. Yagi, E. Ito, T. Kikegawa, and O. Shimomura (1995), Thermal expansivity of $MgSiO_3$ perovskite under high pressures up to 20 GPa, *Geophys. Res. Lett.*, *22*, 1005–1008, doi:10.1029/95GL00584.

Vanpeteghem, C. B., J. Zhao, R. J. Angel, N. L. Ross, and N. Bolfan-Casanova (2006), Crystal structure and equation of state of $MgSiO_3$ perovskite, *Geophys. Res. Lett.*, *33*, L03306, doi:10.1029/2005GL024955.

Vinet, P., J. Ferrante, J. H. Rose, and J. R. Smith (1987), Compressibility of solids, *J. Geophys. Res.*, *92*, 9319–9325, doi:10.1029/JB092iB09p09319.

Wan, J. T. K., T. S. Duffy, S. Scandolo, and R. Car (2007), First-principles study of density, viscosity, and diffusion coefficients of liquid $MgSiO_3$ at conditions of the Earth's deep mantle, *J. Geophys. Res.*, *112*, B03208, doi:10.1029/2005JB004135.

Wang, Y., D. J. Weidner, R. C. Liebermann, X. Liu, J. Ko, M. T. Vaughan, Y. Zhao, A. Yeganeh-Haeri, and R. E. G. Pacalo (1991), Phase transition and thermal expansion of $MgSiO_3$ perovskite, *Science*, *251*, 410–413, doi:10.1126/science.251.4992.410.

Wang, Y., D. J. Weidner, R. C. Liebermann, and Y. Zhao (1994), P-V-T equation of state of (Mg, Fe)SiO_3 perovskite: Constraints on composition of the lower mantle, *Phys. Earth Planet. Inter.*, *83*, 13–40, doi:10.1016/0031-9201(94)90109-0.

Williams, Q., and E. J. Garnero (1996), Seismic evidence for partial melt at the base of Earth's mantle, *Science*, *273*, 1528–1530, doi:10.1126/science.273.5281.1528.

Zel'dovich, Y. B., and Y. P. Raizer (1966), *Physics of Shock Waves and High-Temperature Hydrodynamic Phenomena*, 916 pp., Academic, San Diego, Calif.

Zoysa, E. G. (1985), Colourless enstatite from Embilipitiya, Sri Lanka, *J. Gemmol.*, *14*, 419–425.

T. J. Ahrens, P. D. Asimow, and J. L. Mosenfelder, Division of Geological and Planetary Sciences, California Institute of Technology, Pasadena, CA 91125, USA. (jed@gps.caltech.edu)

D. J. Frost and D. C. Rubie, Bayerisches Geoinstitut, Universität Bayreuth, D-95440 Bayreuth, Germany.